ANISOTROPIC SEISMIC PROPERTIES BENEATH

THE NORTHERN APPALACHIANS: A GUIDE FOR PAST AND PRESENT

DEFORMATIONS WITHIN THE UPPER MANTLE

By

YIRAN LI

A thesis submitted to the

School of Graduate Studies

Rutgers, The State University of New Jersey

In partial fulfillment of the requirements

For the degree of

Master of Science

Graduate Program in Geological Sciences

Written under the direction of

Vadim Levin

And approved by

____

____

____

New Brunswick, New Jersey

October, 2019

ABSTRACT OF THE THESIS

Anisotropic Seismic Properties Beneath

the Northern Appalachians: A Guide for Past and Present Deformations

within the Upper Mantle

by YIRAN LI

Thesis Director:

Vadim Levin

Seismic anisotropy, the directional dependence of seismic velocity, is a proxy for deformation at the depth. Within the Earth's upper mantle, anisotropic seismic observations likely reflect the strain-induced realignment of olivine crystals, which is the major component of upper mantle peridotite. The pervasive mineralogical fabrics form by both the present-day convection of asthenosphere, and the past deformations imprinted in the lithosphere by plate motion and orogenesis. The topography and the surface geology of the Northern Appalachians provide evidences for past tectonic events that had altered the continental margin. Thus, the observation of seismic anisotropy beneath this region should reflect contributions from both the lithosphere and the asthenosphere.

We infer and characterize the seismic anisotropy beneath the Northern Appalachians using the observations of core-refracted shear phases. The multiple provenances of seismic anisotropy likely vary the anisotropic properties along the wave's ray path. As a result, the apparent splitting parameters within each station change with respect to the wave's propagation direction. To effectively compare the directionally

varying splitting parameters across the region, we selected data based on a template list of 61 events with optimized back azimuthal coverage. In addition to single phase splitting measurements, we also obtained station-averaged splitting parameters using Splitting Intensity (SI) technique to consider both split and non-split measurements.

Regionally, the trends of averaged fast axes appear coherent and align with the direction of regional absolute plate motion (average of 249°). The general disparity between the fast axes and the trend of surface tectonic features suggests dominant asthenosphere contribution for the observed seismic anisotropy. The averaged delay times, however, are laterally variable with concentrated localities of smaller delays. The visual comparisons between the datasets of neighboring stations reveal similar splitting patterns with respect to back azimuths and inclination angles, enough for them to be grouped into four regions of distinct anisotropic seismic observations. Such mode of lateral variation suggests that the layered system beneath the region's upper mantle is not uniform but vary geographically and may correspond to localized mantle structures associated with the modification of lithosphere. The inferred domain boundaries correlate only locally with the surficial geological features, and better correlate with the variation of seismic properties in the mantle as suggested by tomography.

ACKNOWLEDGEMENTS

First, I would like to give big thanks to my thesis advisor, Dr. Vadim Levin, for recruiting me into the world of seismology. I was very fortunate to have found the Department of Earth and Planetary Sciences during my time at Rutgers. I would like to thank Dr. Claude Herzberg and Dr. Ying Fan Reinfelder for their time and attention, even though my research topic was out of their realm of specialties.

Thank you to the fellow graduate students, whom I had the pleasure of sharing the experience of graduate school with. My special thanks go to Xiaoran Chen, who has saved me out of many knots that I tied or was about to tie myself into.

I would like to thank Aresty Research Program for initiating and establishing my path in scientific research, and NFS EarthScope for funding my research.

Last but not least, I would like to thank my parents, Sufang and Liming, for their quiet but unfading support and assurance through countless ups and downs.

Table of Contents

List of Figures

1. Introduction

The surface geology of eastern North America records two complete Wilson Cycles that have shaped its lithosphere for more than a billion years. From the assembly of supercontinent Rodinia by ~1.0 Ga to the formation of present-day passive margin flanking the Atlantic Ocean, the region had transitioned through a series of tectonic regimes, including rifting, subduction, and orogenesis. The continental breakup and assimilation of foreign landmasses require plate-scale deformation that had likely left remnant structures within the now-stable continental lithosphere. The detailed characterization of seismic anisotropy provides useful insights for inferring the strength and the scale of deformed structures at depth. Recently, increased station density and duration of data collection has enabled the characterization of finer scale lateral variation of the seismic properties. The improved lateral resolution illuminates potentially ongoing modification of the upper mantle rocks by local geodynamic processes, introducing additional complexities and details to the existing interpretations of seismic anisotropy in the region.

Seismic anisotropy is the dependence of seismic velocity on directionally varying elastic properties. Anisotropic structures within the Earth's upper mantle are commonly associated with the strain-induced alignment of anisotropic minerals (Zhang & Karato, 1995), particularly of olivine. The ductile deformation due to the plate motion and the mantle convection thus produce pervasive mineralogical fabrics that can be detected and characterized using seismic waves that are sensitive to the effects of anisotropy (e.g., Long & Becker, 2010). Additionally, the fabrics of past deformation preserved within the rigid lithospheric mantle, if substantial in strength and spatial dimensions, may also generate local variations in the apparent anisotropic properties. For the eastern North America, the accretion of Gondwana-derived tectonic terranes (Figure 1) makes the contribution of the fossil fabrics likely, due to the amalgamation of the distinct lithospheric mantle fragments belonging to those terranes. Conversely, the modification of the lithosphere following the orogeny may involve processes that overprint the signatures of fossil fabrics. To discern and interpret the geographical variations in the context of both past and present deformations within the upper mantle, we compiled observations of shear wave splitting to take advantage of their desirable lateral resolving ability.

Shear wave splitting is a widely used technique to characterize the upper mantle anisotropy. Early studies (Silver & Chan, 1988; Vinnik et al., 1989; Barruol, 1997, and Levin, 1999, 2000) confirmed the presence and the pervasiveness of seismic anisotropy in the upper mantle of eastern North America. The provenance of anisotropy within the upper mantle, and whether it resides in the asthenosphere or the lithosphere, is an ongoing debate. The relative contributions are often assessed based on the uniformity of the observed parameters across a region; correlations with the surface tectonic features are often cited as the evidence for a strong lithospheric contribution to the inferred anisotropy (e.g. Gilligan et al., 2016). For eastern North America in particular, a study by Levin et al. (2000) proposed a regionally uniform layered system to explain the apparent similarity of observations between different observing locations separated by hundreds of kilometers. Their key finding was that while the measurements at each station varied with respect to the direction of wave propagation, the way in which the data varied with respect to different directions was very similar at all locations that were examined. The pattern of directional variation was cited as the evidence for vertically varying anisotropic properties and was successfully reproduced by forward modelling of wave propagation through a layered system. The layered model proposed by Levin et al. (2000) was later confirmed by Yuan and Levin (2014) using larger data sets, and additional seismic observations indicative of abrupt changes in properties within the upper mantle rock fabrics.

Improved station spacing afforded by the EarthScope USArray Transportable Array (IRIS Transportable Array, 2003) allowed further discernment and characterization of the lateral variation in inferred anisotropic properties. The broad geographical differences in the anisotropic properties were divided into distinct groups within the regional compilation of shear wave splitting observations by studies of Long et al. (2015) and Yang et al. (2017). Further characterization of strong localized variation was enabled by the use of long-running stations in the study by Levin et al. (2018). The improved directional coverage due to an extended period of data collection enabled a more complete sampling of the "fingerprint" of the underlying anisotropy. The stark difference in the observed patterns between proximal stations provides evidence for potentially finer and sharper lateral variations within regions that were previously reported to be homogenous.

In this study, we present a systematic survey of long-running sites with an aim of combining the ability to see the lateral variations with the directional dependence of splitting that was previously taken to signify layering of anisotropic properties. We show that directional dependence of the splitting can be characterized using ample directional coverage, and its geographical variation may serve as an additional basis to further define detailed lateral variations within a region. Similar approach has been adopted by Chen et al. (2018) and Levin et al. (2018) to discern potential areas of unique anisotropic properties based on the specific behaviors of directional variation within the dataset of individual station. We extend this mode of characterization to a broader region to examine the finer-scale lateral variations in detail.

2. Data and Methodology

We performed a systematic mapping of the upper mantle anisotropy with observations of core-refracted shear phases. In an anisotropic medium, a shear wave splits into two orthogonal quasi-shear waves that travel with different velocities (Savage, 1999; Silver & Chan, 1991; Vinnik et al., 1989). For conditions within the sub-lithospheric upper mantle, the fast wave is expected to orient sub-parallel to the direction of maximum deformation (Crampin, 1977; Long & Silver, 2009; Park & Levin, 2002). In addition, a delay accumulates between the arrivals of fast and slow quasi-shear waves in proportion to the strength of anisotropy, as well as to the length of the path which the wave takes to travel through the anisotropic media. The orientation of the fast polarization and the delay time between the two waves can be estimated using the three-component seismograms and are thus conventionally used as the parameters to describe the effects of anisotropy on the shear waves (e.g.; Bowman & Ando, 1987; Silver & Chan, 1991).

The splitting of core-refracted shear phases is commonly used to probe upper mantle anisotropy for the relative ease of attributing their splitting parameters (Long & Silver 2009; Vinnik et al., 1989). Specifically, the phases lose all source-side influence due to their paths through the liquid outer core and assume a predictable polarization after propagating through the core-mantle boundary (Savage, 1999). More importantly, the steep incidence of core-refracted phases provides good lateral resolution that is beneficial for examining the spatial variation of splitting patterns (Long & Silver 2009). The comparisons with other geological observations are often done using pairs of averaged splitting parameters (delay times and fast polarizations) from individual stations (e.g. Long et al., 2015; Yang et al., 2017). While this approach allows associations with broad regional patterns, it may overlook the variations within the datasets of individual stations that potentially reflect the complexity in anisotropic structures (Levin et al., 1999). We attempt to extract more details by comparing sets of individual splitting parameters between each station and assessing the degree of similarities.

We selected 33 stations (Figure 1) from combined networks of permanent observatories (Lamont-Doherty Cooperative Seismic Network, https://ds.iris.edu/mda/LD; New England Seismic Networks (Albuquerque Seismological Laboratory (ASL)/USG, 1994); POLARIS Networks, https://ds.iris.edu/mda/PO; United States National Seismic Network (Albuquerque Seismological Laboratory (ASL)/USGS 1990); Canadian National Seismograph Network (Geological Survey of Canada, 1989)), and Central and Eastern US Network (UC San Diego, 2013) that has retained a subset of USArray Transportable Array (IRIS Transportable Array, 2003) sites for long-term operation. The extended duration of data retrieval was necessary to optimize back azimuthal coverage of the seismic sources and observe the systematic variations of the splitting parameters expected in this tectonically complex area (Levin et al., 1999). The estimated inter-station spacing as small as ~30 km in parts of the region allows us to characterize relatively abrupt lateral variations in splitting parameters that may be attributed to small-scale structures within the upper mantle.

To effectively compare the splitting behaviors between stations, we created a template list of seismic sources using a continuous permanent station (NE.PQI, Figure 1). We selected the sources according to specific thresholds for magnitudes and epicentral distances (Mw. 6.0, and epicentral distances between 85° and 140°) to ensure the visibility of core-refracted phases. The relevant events that occurred between years 2013 and 2017 were then further inspected for clarity of signals. The resulting template consists of 61 visible events with optimal back azimuthal coverage (Figure 2). The lack of events from the east may be attributed to the lack of convergent margins in the respective direction. For each station, we systematically retrieved the seismograms according to the event list to reduce the uncertainty introduced by source effects when comparing the individual splitting parameters. To further minimize bias and ensure systematic data collection, we randomly assigned stations to three analysts and measured in bulk using the SplitLab software (Wüstefeld et al., 2008). We measured all core-refracted phases that were visible in our records, including SKS, SKKS, and PKS phases (called XKS hereafter). We chose to interpret splitting parameters quantified by the Rotation-Correlation (RC) method (Bowman & Ando, 1987) to be consistent with previous studies by Levin et al. (1999;2000;2018). We also compared results with the Minimum Transverse Energy (SC) method (Silver & Chan, 1991) for the purpose of determining measurement type (split or non-split). The consistency or discrepancy of the resulting parameters between the two methods were noted for quality of the measurements. However, given the careful quality control performed prior to data acquisition and the commitment to retain the desired back azimuthal coverage, we interpreted the discrepant splitting parameters as a consequence of complex anisotropic structures (e.g. Long & van der Hilst, 2005; Wustefeld & Bokelmann, 2007) and retained all measured results. The detailed procedure employed to assess the measurement type (split or non-split) and quality closely follows the methodology described in Chen et al., (2018).

For each record, we first examined the signals in both LQT (ray-based) and ZEN (vertical-east-north) coordinate systems to gauge suitable bandpass corners for smoothing the waveforms. The filters were therefore manually adjusted for individual measurements, except for a number of exceptionally clear waveforms for which the filters were not needed. The lower corners were mostly between 0.01 and 0.03 Hz, and the upper corners ranged anywhere between 0.04 and 1.50 Hz. The waveform in the transverse component of the LQT system was assessed in particular for obvious absence of signal that may immediately suggest non-split (NULL) measurements (Figure 3a). For most cases, we determined measurement types and splitting parameters after reviewing complementary observables provided by SplitLab, including particle motions, the transverse waveforms before and after correction for anisotropic effects, and the characteristic discrepancy of splitting parameters between the RC and the SC methods. The rectilinear particle motion (Figure 3b), and the exceptionally small delay time yielded by the RC method coupled with the exceptionally large delay time (reaching the maximum value assigned for grid search) yielded by the SC method were the key determinants for NULL measurements. Conversely, the presence of signals in the transverse component, as well as the elliptical particle motion (Figure 3b) were noted for split measurements. We saved the results after examining the persistence of characteristic observations and stability of parameter values with different time windows selections and filters.

In addition to characterizing the patterns of the individual measurements, we also obtained station-averaged splitting parameters to characterize the regional trends and verify the observations reported by previous studies. We estimated averaged splitting parameters using the multichannel approach proposed by Chevrot (2000) to ensure the incorporation of NULL measurements during the computation of averaged splitting parameters. The method utilizes the sinusoidal pattern of splitting intensity values (SI) expected as the function of varying back azimuths and delay times, described in the relationship;

$$SI = \delta t \times \sin [2(\varphi_o - \varphi)],$$

where δt is the averaged delay time, φ is the averaged fast axis polarization, φ_o is the back azimuth, and SI is the amplitude of transverse signal relative to the time derivative of radial signal (Chevrot, 2000). We adopted the modified SplitLab packaged with the function to calculate SI values used in Deng et al. (2017) to obtain individual measurements. All measured SI values from each station were collectively fitted to a sinusoid by least square minimization method, from which the splitting parameters (delay times and fast polarizations) for a single layer of anisotropy were derived using the formula above (Figure 3d). We defined the uncertainties for both splitting parameters as the highest and the lowest values that fell within 95% confidence interval of the mean. To verify the reliability of the multichannel method, we also individually obtained arithmetic means of individual delay times and fast polarization orientations for all split measurements within a station. The standard deviations were defined as the uncertainty for the arithmetic means. The two sets of station-averaged parameters, and the directional variations of individual splitting parameters within each station (Figure 3c), form the dataset that we will characterize and interpret in the subsequent sections.

3. Results

In total, we accumulated 1393 pairs of new splitting parameters from the 33 selected stations in the Northeastern Appalachians and adjacent Grenville Province. Of those, 500 pairs were deemed NULL based on the criteria described in the Methodology and Data section. Although we strived for the clarity of waveforms and the uniformity of events measured at each station, about 30% of the total expected records were neglected due to excessive noise or instrument malfunction. In the end, the numbers of measurements per station range between 19 and 78, with 20 of the stations having more than 35 measurements.

Figure 4 shows examples of good single-event splitting captured by nearly all of the stations. Generally, the splitting parameters yielded by a single event show regionally coherent fast polarization. While the delay times are laterally variable, the patterns in which the delay times vary over the study area are remarkably similar between the two different events with similar event back azimuths, namely NNE (Figure 4a, 4b). In particular, the largest delay times and SI values concentrate at the northern Maine and northern New York. Elsewhere, the measurements show relatively small delay times or were deemed non-split, accompanied by corresponding small SI values. The overall fast polarization and SI values, and the spatial variation of delay times changes dramatically when the same region is sampled by waves propagating from NW (Figure 4c). Specifically, the fast polarizations shift to orient dominantly WNW-ESE, and the largest delay times are instead recorded in southern Canada and southern Maine. All stations thus show evidence for directional variation of splitting parameters. As such, the characterization of regional splitting parameters based on a limited range of back azimuth may yield biased descriptions of the underlying anisotropy.

In order to characterize the splitting patterns with optimal station density, we incorporated the stations from previous affiliated studies that followed similar procedures of data retrieval and classification. Namely, we included the data from stations PQI and GGN featured in Li et al. (2017) and six stations (PKME, HNH, MCVT, NCB, QUA2, and UCCT) analyzed in Levin et al. (2018). We describe both the regional patterns of station-averaged splitting parameters, as well as the localized regions of distinct splitting patterns defined through qualitative and quantitative examinations of splitting parameters within each station.

3.1. The Regional Trends of Station-Averaged Splitting Parameters

Figure 5 shows the two pairs of averaged splitting parameters at each station. The station-averaged fast polarization directions obtained using the SI method of Chevrot (2000) show regionally coherent orientations, with values ranging between azimuths of 69° and 96° (Figure 6a). The dominant orientation as seen in the histogram distribution varies according to the arbitrary choice of bin sizes. While the dominant orientation approaches the arithmetic mean with smaller number of bins, it generally remains between the range of 70° and 80° azimuths, where the bin size allows for a unimodal and slightly skewed distribution. The values obtained by the splitting intensity method are also remarkably similar to the values obtained by the simple averages of fast polarizations, which only consider the measurements that were deemed split (Figure 6b). While the peak resides in the same range as the distribution yielded by the splitting intensity technique, the distribution of simple averages appears to show peaks at the center of the distribution due to the wider range of values, ranging between 61° and 106° azimuths.

For both averaging techniques, the peaks of their respective distributions lie consistently clockwise of the region's absolute plate motion (approximately 249° azimuth), obtained from the HS3-NUVEL 1A plate motion model based on a hot spot reference frame (Gripp & Gordon, 2002). This systematic mismatch between the absolute plate motion and the dominant fast polarization orientation is further reinforced by the observation of NULL (non-split) measurements (Figure 6c). Generally, the waves coming from the back azimuthal range in alignment with the fast polarization orientation within the anisotropic media are expected to yield NULL measurements (e.g., Savage, 1999). In the back azimuths sampled by our results, the NULL measurements concentrate in WSW, with a dominant peak appearing between 260° and 270° azimuths (80° to 90° azimuth in modulo 180°). Again, the dominant NULL-yielding back azimuthal range is in better agreement with the mean station-averaged fast polarization orientations than the direction of the regional absolute plate motions. Altogether, the similarity of dominant station-averaged fast polarizations and NULL-yielding back azimuths form an observation consistent with a single layer of anisotropy, in which the orientation of maximum deformation mismatch systematically from the regional absolute plate motion.

The correlation between the fast polarizations and the trend of the Appalachian topography is unclear. Both distributions of station-averaged fast axes are well out of the range for the orientation of orogenic trend, which rotates clockwise from about 10° azimuth in the southern end to approximately 40° azimuth in the northern end of our study area (Figure 1). Noteworthy though, is the presence of some NULL measurements falling within the range of back azimuth in alignment with the above orientation of orogenic trend.

The average delay times are laterally variable with a discernable regional trend evident in both sets of station-averaged values (Figure 7a). Both sets of delay time distributions show increase from the average of 0.5 seconds in the southern end to the maximum of 1.38 seconds in the northern end of our study area (Figure 7a). Small local anomalies are also present, as evidenced by the abrupt reduction of delay times near the latitudes of 42 degrees north and 44 degrees north, most clearly captured by the SI technique (Figure 7b) and to a lesser extent by the simple averaging (Figure 7c). The locations correspond to the splitting parameters from stations L64A and HNH respectively (Figure 5), which are distinguished by the high proportions of NULL measurements observed from all sampled back azimuths.

The lateral variation of the delay times manifests differently between the two averaging techniques. As with the case of fast axes orientations, the delay times obtained by the simple averages show relatively smooth, unimodal distribution (Figure 8b). While stations in the south (40° to 44° latitude) show smaller uncertainties than those in the north (44° to 48° latitude), the regional trend of delay times captured by simple averaging is best described as a gradual increase from the south to the north, due to the large error bars and the significant overlap between adjacent stations (Figure 7c). In contrast, the values obtained from the SI technique (Figure 8a) show a wider spread of delay times, ranging from values as small as 0.1 seconds obtained at stations like L64A and HNH, to as large as 1.38 seconds obtained at station G65A in the northern Maine. While one peak forms near the arithmetic mean of about 0.76 seconds, the distribution is hardly unimodal, but better characterized as having multiple peaks at different delay times (Figure 8a). Such distribution obtained by the SI technique suggests that lateral variation of delay times may be spatially discrete. The regional trend of delay times obtained by the SI technique (Figure 7b) is also consistent with this view. Their uncertainties of individual station-averaged delay times are much smaller than those obtained by simple averaging. As such, the regional trend may also reveal two potential populations of delay times, in addition to the sharp local reduction delay times at stations like HNH and L64A. Specifically, the stations in the latitude range of 40° to 43° collectively show smaller delay times (average of 0.7 second) than those in the latitude range of 44° to 48° (average of 1.0 second).

3.2. The Regional Characterization of Traits Observed in Stereonet

All stations show variation of individual splitting parameters that are dependent on the back azimuths and the incidence angles of the phases. Motivated by the observations from stations like HNH and L64A, which displayed both anomalous averaged parameters as well as the characteristic patterns collectively formed by individual splitting parameters, we further investigated the splitting patterns within the dataset of each station to see whether the localized splitting anomalies may be better characterized by a systematic variation of the splitting pattern as a function of back azimuths. By visually comparing the appearance of splitting patterns in the stereonet (Figure 3c), we find that neighboring stations generally share similar splitting characteristics. We grouped the stations into four anisotropic domains based on a combination of qualitative traits and reasonable geographical proximity. The specific criteria used are:

1) the relative amount of NULL measurements in the dataset of individual stations,
2) the back azimuthal distribution of the NULL measurements (dispersed vs. concentrated),
3) the variation of fast axes orientation and delay times with respect to the varying back azimuths and inclination angles, and
4) the averaged parameters obtained from the split intensity method.

The back azimuthal variations of splitting parameters are likely indicators of complex anisotropic structures (Levin et al., 1999; Savage, 1999), consisting of vertically or laterally varying anisotropic properties in the sample region that likely deviate from the simple cases of anisotropy (single layer, horizontal fast axis) implicitly assumed in the quantification techniques used by the SplitLab software. We chose to examine the parameters observed by Rotation-Correlation method after Bowman and Ando (1987), for it yields delay times that are compatible (approximately 1 second given 4% of anisotropy) for the thickness of the lithosphere beneath this study region, as well as intuitively small delay times for the cases of NULL measurements. Although the method is expected to yield fast axes that are systematically 45° away from the incident back azimuth for complex anisotropic structures (Wüstefeld et al., 2008), the extent and patterns to which the splitting parameters fluctuate with respect to the back azimuth appear to change depending on how the underlying anisotropy varies with respect to the depth. Because we obtained each measurement through a predefined procedure of quantification and classification, we regard the differences in splitting patterns as the indications of different anisotropic structures manifested as a result of this systematic mode of data treatment. The notable characteristics of each domain are described in the following section. Domains are named with arbitrary color codes and were defined purely on the basis of observed seismic anisotropy. Spatial correlations of domain boundaries with other observables, such as the surface tectonic features and the distribution of seismic velocities at depth, are addressed in the Discussion section.

3.2.1. Description of Anisotropic Domains

In this section we provide a detailed description of traits that we used to define the boundaries of individual domains in Figure 9. Representative stereonet diagrams are shown in Figure 9, and diagrams for each site are presented in an electronic supplement, Figures S1 to S33.

3.2.1.1. Yellow

The most distinct within our study region is the yellow domain. Represented by the observations from stations such as L64A and HNH, it is characterized by the high proportion of NULL measurements within the datasets of individual stations (Figure

10a). Compared to regional average of about 35% of individual splitting parameters being NULL, the stations enclosed by the yellow domain have proportions up to a maximum of 83%. The strong fluctuation of fast polarization orientations, evidenced by the large (up to 40°) standard deviation (Figure 10b), may be attributed to the sampling bias due to the low number of split measurements. However, the split measurements appear remarkably similar between the stations when the NULL measurements are removed. The drastically small standard deviation for the delay times (Figure 10c) may also be attributed to the same sampling bias. Although the proportions of NULLs decrease towards the rim of yellow domain, their averaged delay times are small compared to the surrounding stations for both averaging techniques. The sharp contrast of the averaged delay times with the green and blue domains, as well as the relatively high NULL proportions, allow them to be included in this domain.

3.2.1.2. Red

The red domain, southwest from the yellow domain, encompasses the locality of second smallest averaged delay times. While this domain also exhibits relatively high NULL proportion within the study region, its averaged NULL proportion is 39%, only slightly higher than the regional average, with the maximum of about 53% at station PANJ in the northern New Jersey. Additionally, the back azimuthal distributions of the NULL measurements are less dispersed, with a discernable dominant NULL direction from WNW, as well as clusters of NULL measurements in the north and the south. The red domain is distinguished from the green domain to its north by the higher proportion of NULL (Figure 10a), as well as the degree to which the individual splitting parameters fluctuate with respect to the incident back azimuths. Specifically, the delay times of red domain remains relatively constant with respect to the incident back azimuths, as evidenced by the small standard deviations of delay times (Figure 10c). In contrast, the fast polarizations fluctuate more extensively, as evidenced by the collectively higher standard deviation (Figure 10b), as well as the distinct bimodal distribution of the individual fast axes when shown in a histogram (e.g.; Figure A2c, A27c, A29c).

3.2.1.3. Green

The stations in the green domain collectively have lower numbers of NULL measurements compared to the domains further south (Figure 10a). They are most distinguished by the concentration of NULL measurements from WNW (Figure 9a), as well as the limited fluctuation in the range of fast axes, as evidenced by the smaller standard deviation compared to the surrounding domains (Figure 10b). The differences are evident with comparison to the stations in the red and yellow domains, and the majority of stations blue domain to the east. The delay times, on the other hand, show stronger fluctuation than in the more southern domains. Qualitatively, most stations grouped into the green domain show the distinct reduction in delay times from the northeastern quadrant towards the northwestern quadrant of the stereonet (Figure 9a). The consistency of splitting patterns between different stations is in part supported by the relatively similar values of standard deviations within the green domain for both the fast axes orientations and the delay times.

3.2.1.4. Blue

The blue domain contains the most diverse splitting patterns, for both station-averaged and individual parameters. Though it shares similarities with the red and green domains, the blue domain is distinct for possessing strong fluctuations for both the fast polarization and the delay times, while the other two domains are characterized by having only one parameter fluctuating more strongly than the other. Collectively, the individual fast polarizations in the blue domain form a bimodal distribution in the histogram (e.g.; Figures A6c, A7c, A13c, A14c), and the delay times encompass a large spread. The most prominent examples of such qualities can be observed in the northern Maine (stations F63A and G62A, Figure 1). The splitting patterns are variable from the center to the rim of domain. It is best differentiated from the northwestern stations (stations LATQ and MNTQ, Figure 1) and the yellow domain by the sharp contrasts of averaged fast polarizations and the proportion of NULL measurements within each station, respectively. Similar to the green domain, the blue domain has a narrow range of back azimuths in the WNW that yield NULL measurements. Furthermore, permanent stations like PQI and PKME from Levin et al. (2018), which include more events, show a wide cluster of NULL measurements in the northeastern quadrants, corresponding to 0° to 45° azimuth.

Due to the limited number of sites to the north of Adirondacks, it is difficult to declare the region encompassed by the two stations (LATQ and MNTQ, see their diagrams in the supplement) as a domain. However, we note that the differences of splitting patterns between these stations and the stations within the surrounding domain are distinguishable. In particular, the characteristic drop of the delay times yielded by the northwestern events, shared by the stations in the green domain, is absent. Their delay times do not show systematic reduction for all of the sampled back azimuths. More characteristic to this region is the distinctly E-W oriented fast polarization compared to the relatively NE-SW fast polarization of the green and blue domains. The relatively small standard deviation of the spread (Figure 10b), particularly in comparison with the stations in the blue domain, suggests that the population of sampled fast orientation systematically shifts to E-W within this region. Further examination and verification of potentially different anisotropic properties beneath this region may be possible by incorporating more stations.

3.2.2. Domain-wise Fit to an Anisotropic Model by SI Technique

To verify the similarity of splitting behaviors within each domain, we tested the domain-wide fit of individual splitting intensities to a common sinusoidal pattern predicted by a particular anisotropic model (Figure 11). Conversely, we also estimated a best-fit sinusoid for the same collection of splitting intensity values using least squares minimization. The similarity between the predicted and the fitted sinusoids reinforces the stability and self-consistency within the combined datasets, as well as provides a quantitative means for constraining the averaged anisotropic strength beneath each domain. The averaged delay time δt is constructed on the basis of values returned by the Rotation-Correlation method (see Methods section). Other methods of estimating shear wave splitting tend to yield larger delay values in cases where data are not ideal (Wustefeld & Bokelmann, 2007). The compatibility of the RC method and the Splitting Intensity technique is another reason for us to prefer its values in this study.

For each anisotropic domain, the two sinusoids are generally in good agreement, as suggested by the general overlap of the sinusoids and the similar averaged splitting parameters estimated by both the SI technique as well as the simple averages. The yellow domain shows the most mismatch between the two sinusoids (Figure 11d). The discrepancy may be explained by a large proportion of measurements defined as NULL. They are not included in the computation of averaged splitting values obtained by the RC technique, but their SI values are included in the estimate of best-fitting sinusoid. The lower amplitude of the fitted curve obtained by fitting SI values indicates that simple averaging that only considers the split measurements may overestimate the delay times in the cases of abundant NULL measurements, as observed in the yellow domain.

3.2.3. Geometries and Characterization of the Inferred Domains Boundaries

The geometries of the domain boundaries are inferred between the groups of stations that show similar splitting behaviors according to our quantitative and qualitative classification schemes. The boundaries can therefore be altered, and more detailed structures may be unraveled using different sets of classification criteria and station distribution. The nature of the transition may also contribute additional complexities for determining the domain geometries.

Within our study area, we observe both sharp transition of splitting behaviors, as well as gradual occurrences and disappearances of certain traits that result in provisional boundaries. For instance, the region enclosed by the yellow domain shows consistent splitting behaviors that are clearly different from the surrounding domains, as supported by the distinct values in all featured quantitative measures. Meanwhile, the shift between the red and the green domains appear to occur over greater distances, with some transitional stations such as L59A and TRY in the southern New York that contain traits that are characteristic to both green and red domains. Although the boundaries may be better resolved by both increased station density and data number, it is also possible that the nature of the boundaries reflects the properties and arrangements of the underlying Earth structures themselves, which are not necessarily laterally discrete. What should be undisputable from our dataset, however, is the presence of well-defined regions of systematic splitting behaviors that are describable with the observations known to vary according to complex anisotropic structures. Despite the variable width of domain boundaries, the distances over which the patterns systematically change between the groups of stations are relatively short compared to the aerial extent encompassed by the stations that share common characteristics. Examination of splitting patterns within each domain may uncover potential details that are otherwise masked by the seemingly coherent regional trends of the averaged splitting parameters.

4. Discussion

4.1. Comparison with Previous Studies

Multiple studies (e.g.; Long et al., 2015; Wagner et al., 2012; Yang et al., 2017) have characterized seismic anisotropy beneath the eastern North American margin in detail using shear wave splitting method. While various sources of anisotropy and mechanisms are introduced to explain the heterogeneous splitting patterns along the margin, a number of converging views are achieved together with constraints provided by other means of probing seismic anisotropy and velocity boundaries at depth. Generally, the widespread similarity of the orientation of fast polarization suggests a pervasive source of anisotropy due to the ongoing deformation within upper mantle due to the flow of asthenosphere, and the laterally variable splitting patterns suggests smaller-scale, shallower source of anisotropy, possibly introduced by “fossil” fabrics frozen within the lithosphere from past deformations. In addition, evidence for multilayered anisotropy has been inferred, both through back azimuthal variation of the splitting patterns within a station (Levin, 1999, 2000), as well as anisotropic velocity boundaries detected through receiver functions (Yuan & Levin, 2014).

The results from our study are compatible with the observations reported by previous studies performed in the same region (Figure 12). The trends of fast polarizations measured in this study (E-W, and ENE-WSW) and their general uniformity over the study region is consistent with the finding of other studies that have characterized the lateral variation of splitting patterns throughout the eastern North America (Long et al., 2015; Yang et al., 2017). In particular, our study regions fits into Region A defined by Long et al., (2015) which was grouped on the basis of regionally consistent, E-W (average of 77°) trending fast polarization orientations and its smooth lateral variation. Our delay times also show similar patterns of spatial variation, though with discrepancy for the overall range of delay time values between this study and the previous studies. Locally, the largest delay times are observed in the northern Maine, where individual splitting parameters as high as 4.0 seconds are reported by previous studies (Chen et al., 2018; White-gaynor & Nyblade, 2017). Similarly, the reported delay times near the southern end of the study area is smaller, with most studies showing values smaller than 1.0 second. While our delay time values agree with this trend, the range of values reported by our study are significantly smaller, with a maximum delay time of under 1.4 seconds in the northern Maine.

With good back azimuthal coverage, we also find directional variation of the splitting parameters at all of our stations, consistent with the vertically varying anisotropic properties reported for most regions within the eastern North America. The complex anisotropy is known to cause discrepancies between the apparent splitting parameters quantified using different techniques (Long & van der Hilst, 2005). Even though the directional fluctuation of individual delay times is expected, our highest delay times obtained using the RC and the SI methods do not exceed 2.5 seconds, smaller than the maximum of 4 seconds obtained by Transverse Component Minimization method (Silver & Chan, 1991) used in other studies. The discrepancies of splitting parameters may thus reflect the response of different techniques to observed waveforms reflective of complex anisotropy. Although the different measured values complicate the comparison between the results of this study and the previous studies, all data sets nonetheless seem to report a similar geographical pattern of splitting parameters, including the general coherency of averaged fast polarizations and lateral variation of delay times. In addition, the agreement between our two sets of splitting parameters, yielded by SI technique and RC technique, provides assurance for the reliability of our data.

4.2. Comparison with Other Geological and Geophysical Observables

The tectonic terranes presently exposed in the Northern Appalachians can be linked to episodes of crustal deformation from multiple collisional events that comprise the Appalachian Orogeny (Hatcher, 2010). Geological evidence defines three main orogenic events; the accretion of a volcanic arc during the Ordovician Taconic orogeny, accretion of microcontinents during the Devonian Acadian orogeny (Hibbard, 2006), and finally the culminating continental collision during the Permian Alleghenian orogeny. The finer terrane boundaries on the surface are delineated by differences in lithologies and detrital zircon signatures that are interpreted on the basis of subduction-related magmatism and different sediment provenances pertaining to the origin of specific terranes (Hibbard & Waldron, 2009; Karabinos et al., 1998). The increased details of geological and geochemical observations at the surface are reconciled by invoking contributions from deep structures, such as changing subduction polarities and slab detachments, providing implications for what structures should exist at the depth. The resulting heterogeneity of anisotropic properties from the deformation within the upper mantle is likely to be captured by the lateral variation of shear wave splitting observations. However, as illustrated by single-event splitting maps in Figure 4, the observed lateral variation reflects both the scale of the anisotropic structures at depth and the direction of illumination by shear waves. Consequently, it is important to include directional patterns in splitting values (e.g.; Figure 9) in the definitions of anisotropic domains that many correspond to tectonic terranes or features of the upper mantle structures formed by past tectonic episodes.

The attempts to discern subsurface volumes with anisotropic properties, and by extension the relative contributions from the lithosphere and the asthenosphere in the apparent observations, have in part relied on comparisons with other geological and geophysical observables. The parallelism of tectonic faults and orientation of fast polarizations of split shear waves may signify substantial lithospheric contribution to the apparent splitting. Furthermore, the sharp lateral variation observed between two closely spaced stations can suggest changes in anisotropy that are relatively closer to the surface (Aragon et al., 2017). Here we compare our station-averaged splitting parameters and the spatial distribution of our station groups with surface geology (Figure 13a) and shear wave velocity distribution based on the model of Shen and Ritzwoller (2016) at the depth slice of 90 km (Figure 13b). The lithosphere-asthenosphere boundary in Northern Appalachians is seen at 85-100 km depth (e.g.; Abt et al., 2010; Rychert et al., 2007) thus variations in velocity seen in this depth slice should be representative of the overlying lithospheric structure.

At the first glance, the obvious mismatch between the averaged orientations of fast polarization and the trends of tectonic features is striking. With the possible exception of a small area in southern Quebec and northwestern Maine, the fast polarizations remain oblique to the trends of terrane boundaries and the Appalachian suture and do not imitate their curvatures as they change from south to north (Figure 1 and Figure 13a). However, this mismatch needs to be considered in the context of directional variability in splitting parameters seen at most sites of the region. As explored in earlier papers by Levin et al., (1999;2000) and also by Yuan and Levin (2014), the true orientation of the anisotropic fabric at various depth levels is guaranteed to be different from the average. It is therefore possible that lithospheric mantle of the region does contain anisotropic textures aligned with terrane boundaries, though formal modeling effort is needed to ascertain it. On the other hand, the geometry of domain boundaries shows some correlations with the surface geology. In particular, the Adirondack mountains in the northern New York correspond spatially to the green domain. The characteristic appearance of stereo plots in this domain suggests a localized volume within the underlying upper mantle that possess a distinct arrangement of vertically varying anisotropy. The distinct character of the Proterozoic Adirondack mountains is not surprising, as this is the only area in our study that belongs to Laurentia and has not been affected by the orogenic processes during the assembly of Pangea. Consequently, the lithosphere of this area and the anisotropy-forming fabric within in are at least ~1 Ga old (the age of the Grenville Orogeny, Hynes & Rivers, 2010). To explain the timing of emplacement of anorthosite bodies in the Adirondacks, Mclelland et al. (2010) proposed an episode of lithospheric foundering and replacement, a process likely recorded in the residual lithospheric fabric. Additionally, the lithosphere of this domain may be experiencing a modern-day alteration, as suggested by the surface wave imaging by Yang and Gao (2018).

In the domains within the Appalachian orogen (red, yellow, blue) there is no apparent correlation between averaged splitting parameters and individual terranes (e.g. Avalonia, Gander) that represent different tectonic units assembled in the Paleozoic. Instead, similar patterns of splitting enclose areas with multiple terranes identified by surface geology. This likely points to the lithospheric, or deeper, origin of the differences in their splitting patterns. This is especially clear in Maine where individual tectonic units of the Appalachians are significantly wider relative to their extensions further south (cf. Figure 1, Figure 13a), but show high similarity in anisotropic signature. The vertical extent of the lithosphere is similar in these domains (Abt et al., 2010), however they belong to two parts of the Appalachian Orogen that may have experiences different tectonic histories (e.g. Hatcher, 2010). Distinct lithosphere structure may be the cause for the clear difference in strength of the spitting signal, ~0.5 s in New Jersey vs over 1 s in Maine. However, the local variation in sub-lithospheric flow may also play a role, especially considering the previously documented association of the yellow domain with a deep-seated (100 – 300 km) North Appalachian Anomaly (NAA) (Schmandt and Lin, 2014; Menke et al., 2016; Levin et al., 2018).

The boundaries of the yellow domain appear to be aligned better with the slow feature at greater depths seen in most tomographic studies with sensitivity to the 50 – 150 km range (Shen & Ritzwoller, 2016; Yang & Gao, 2018; Figure 13b). The feature is located beneath Vermont and New Hampshire, and spatially coincides with a deeper NAA anomaly. The near-absence of splitting in this domain implies the lithosphere is lacking a well-developed texture, a significant localized difference from areas to both north and south that share the Paleozoic tectonic history with it. A possible cause of this local anomaly in both seismic velocity (slow) and anisotropy (absent) may be the influence of the deeper asthenospheric upwelling proposed by Menke et al., 2016 and Levin et al., 2018. It is interesting to consider the possibility that lithosphere alteration by the passage of a hot spot (Eaton & Frederiksen, 2007; Sleep, 1990) left an imprint that presently guides the upwelling to this region.

Other parts of the region also show a degree of correlation between the anisotropic signature and seismic velocity at lithospheric depths. Specifically, the green domain over the Adirondacks seems to better match the regions of intermediate velocities adjacent to the slow anomaly. The stations of red domain and the two sites within the Grenville province, match with the regions where the velocities are relatively high. The better correspondence between the domain geometries and the velocity structure at the depth of 90 km suggests that the different domains may reflect the differences in the seismic properties within the lithospheric mantle or near the lithosphere-asthenosphere boundary of the region. Consequently, the apparent variation of the seismic velocities determined under the assumption of isotropy may be controlled in part by the variation of anisotropic properties.

4.3. Vertically Incoherent Deformation

The observations of shear wave splitting from the adjacent segments of the Appalachian Mountains, including Newfoundland, Canada by Gilligan et al. (2016) and southeastern United States by White-Gaynor & Nyblade (2018) and Long et al. (2015) report strong correlation between the orientations of averaged fast polarization and the surficial tectonic and topographic features. The similarity between the fast polarization and the tectonic features is cited as evidence for strong relative contributions from the fossil lithospheric fabrics, as well as for coherent deformation of the crust and the lithospheric mantle (Silver, 1996). For the region investigated by this study, however, we do not observe this clear correlation with neither the regional topography nor the well-defined terrane boundaries (Figures 1, 13A).

As discussed in the previous section, the lithospheric contribution to the apparent splitting we have measured is undisputable. However, as we do not see the match between the average splitting directions and the features of surface geology, we conclude that the lithosphere must have a fabric distinct from that of the shallow crust. This in turn implies vertical decoupling of the deformation between the lithosphere and the crust during the Appalachian Orogeny which was the last tectonic event to affect the entire region. Additionally, the strong correlation of average fast polarizations to the APM throughout the region suggests that a dominant contribution to the splitting pattern is from plate motion relative to the asthenosphere, a finding similar to that of Long et al. (2015).

The varying relationship between the averaged fast polarizations and the surficial geological features along the Appalachian Mountains may be listed as yet another feature of the dichotomous characteristics that are persistently noted between the northern and the southern segments of the Appalachian Mountains. The contrasting geographical distribution of the timings of deformation (Hatcher, 2010) and the different delineation of terranes allude to potentially separate tectonic histories of northern and the southern Appalachians (e.g., Hibbard et al., 2007). Because the phases used for shear wave splitting should have similar sensitivity for the regions within the upper mantle, the different patterns of the averaged fast polarizations may reflect the differences of underlying anisotropic structures that may pertain to the individual tectonic histories between the southern and the northern segments. Notably, the apparent similarity between the fast polarization and the tectonic features in the southern Appalachians, reported in both Long et al. (2015) and White-Gaynor and Nyblade (2018), is based on the averaged splitting parameters derived using relatively short (2 years) periods of observation. As the experience of our study with longer data sets shows, the averages obtained by limited back azimuthal sampling may yield different values. While the apparent differences of the averaged fast polarizations between the northern and southern Appalachians may be noteworthy, meaningful comparison and characterization with the observations reported by this study require extending the same mode of analysis into the southern Appalachians.

4.4. Non-uniform Upper Mantle Anisotropy, and the Motivation for Forward Modeling

The weaker lithospheric contributions are difficult to quantify and characterize by simply using the station-averaged splitting parameters because the signatures indicative of finer-scale lateral differences may be disregarded by the averaging procedures. The local variations of splitting patterns detected through our procedure allow consideration of all individual splitting parameters and characterization of heterogeneous splitting behaviors at a finer scale than the previous studies. With improved back azimuthal coverage, we show that directional variation of the splitting parameters is not uniform throughout the Northern Appalachians. Rather, the region can be divided into discrete areas that show distinct patterns of directional variation.

In addition, all stations within each respective area share a similar splitting behavior, likely modulated by a common source of vertically varying anisotropy. The transitions between the domains also occur over shorter distances than the areas encompassed by the individual domains. The sharp boundaries, depending on the scale of the observed lateral variation, may be attributed to processes and structures proposed at various scales and depths, including remnant tectonic features, local geodynamic processes, or the topography of the lithosphere-asthenosphere boundary.

Our finding of at least four distinct anisotropic domains in Northern Appalachians contradicts the earlier publications by Levin et al. (2000ab) that argued for a uniform regional layering of anisotropic properties. The key difference between those studies and the present one is in the quantity of data, both in terms of the length of observation, and especially in terms of the lateral sampling of the region.

The poor depth resolution of shear wave splitting method poses difficulties for attributing the anisotropic structures to specific provenances. Forward modeling is required to better describe and constrain the vertical variation of anisotropic properties. However, the attempts to model the station-averaged splitting parameters may result in non-unique outcomes due to the tradeoffs between the anisotropic strength and the thickness of the layers. The model constrainable by the station-averaged splitting parameters, therefore may be only sufficient for deeper, more pervasive sources of anisotropy. The evidence for regional variation of the splitting behavior, observed through the individual splitting parameters as done in this study, provides concrete incentives to vary the anisotropic models locally to better reproduce the observation obtained at each site. The sharp lateral variation enables the modelling of shallower features, and the specific combination of individual splitting parameters in the dataset of each station provides more quantitative features to discern the wellness of fit between different models.

Figures

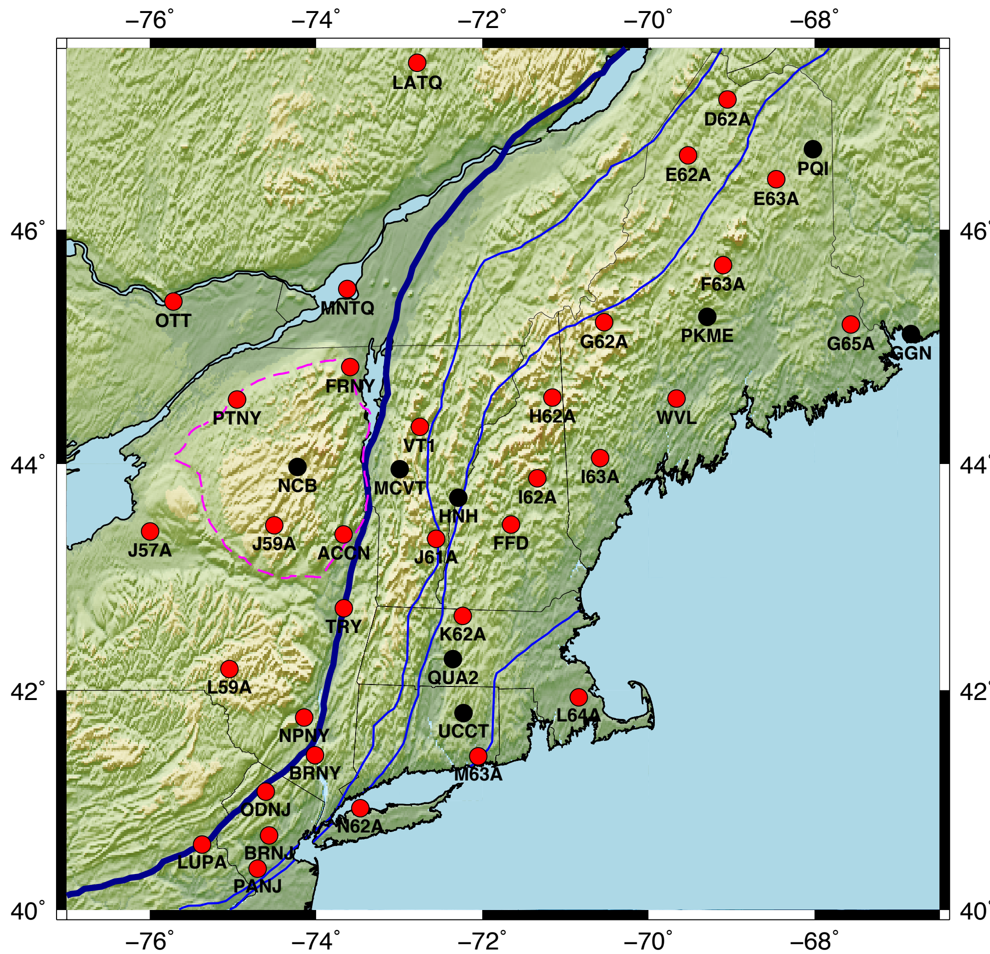

Figure 1: The distribution of featured stations across the northeastern Appalachians. The red circles indicate long-running stations that yielded new datasets for this study. The black circles indicate the stations included from Levin et al. (2018) and Li et al. (2018) to improve the station density. Station PQI, marked in yellow, was used to create the template event list for homogenizing the datasets. The blue lines estimate the major geological boundaries pertaining to the tectonic history of the region, modified from the United States Geological Survey basement domain map (http://mrdata.usgs .gov./ds-898). The thick blue line indicates the Appalachian Front, while the thin blue lines are terrane boundaries separating Taconic Belt, Gander, and Avalonia, respectively from west to east. The magenta dashed line outlines the aerial extent of Adirondack mountains.

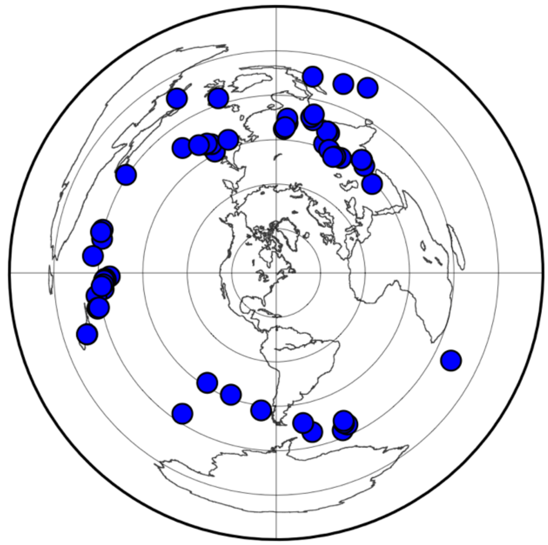

Figure 2: The distribution of 61 selected events with respect to our study area (center). The grey circles indicate the aerial extent encompassed by discrete epicentral distances, starting with 0° at the center and increasing with increments of 30° towards the rim.

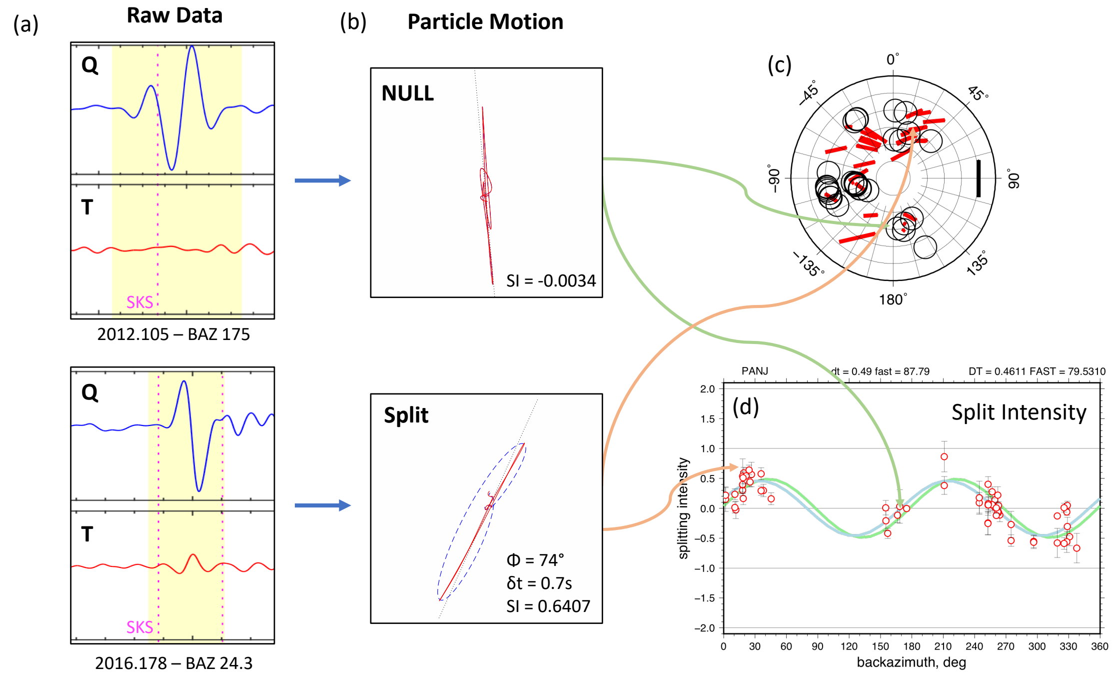

Figure 3: The workflow to obtain the datasets used to characterize laterally varying splitting behaviors. The example is from the station PANJ. a) the recordings of the SKS signals, rotated to LQT coordinate system. The blue line shows the radial component, and the red line shows the transverse component. b) the particle motion of the waves; the top shows a wave that was not split (NULL), forming a rectilinear particle motion, and the bottom shows a split wave, showing an elliptical particle motion. c) The example of stereonet showing the dataset of a station. The circles are NULL measurements and the lines are split measurements, with lengths proportional to delay times and the orientations aligned with those of the fast axes. The data closer to the center of the stereonet has steeper inclinations. d) The sinusoidal curves calculated from the splitting intensities of each event measurement. The blue line is the sinusoid that best-fit the split intensity values, and the green line is the sinusoid predicted from the averaged splitting parameters.

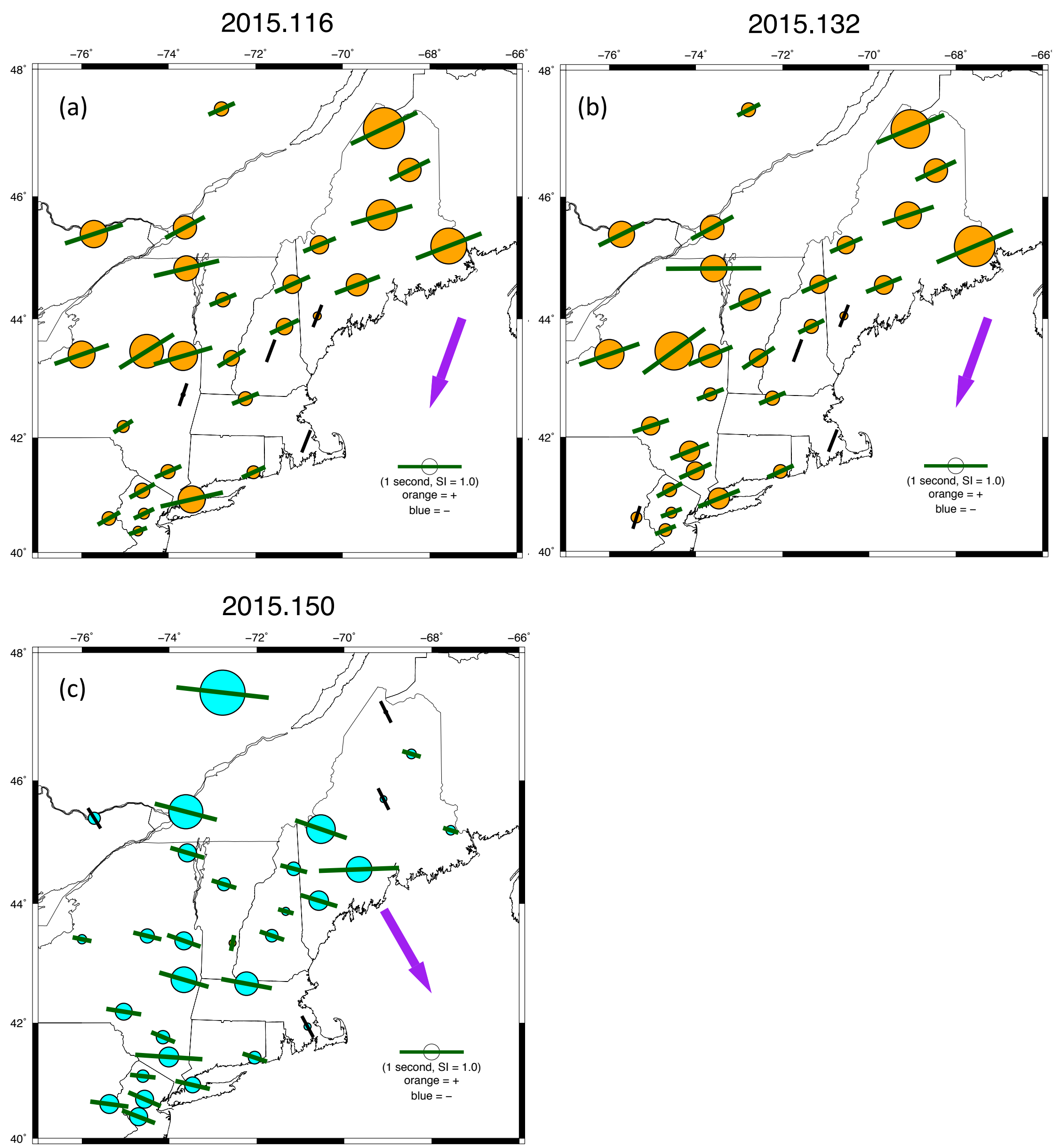

Figure 4: Example of individual splitting parameters and splitting intensity (SI) yielded by three events that occurred in 2015, labeled with respective Julian dates. The green bars align with the estimated fast polarization orientations and are scaled in proportion to the delay times. The purple arrows indicate the direction of wave propagation. The circles are scaled proportional to the magnitude of SI values; the orange circles indicate positive values and the blue circles indicate negative values. Event 2015.116 (a) and event 2015.132 (b) share similar direction of wave propagation, and consequently a very similar splitting pattern. Event 2015.150 (c) propagates from NNW, and the splitting pattern is starkly different.

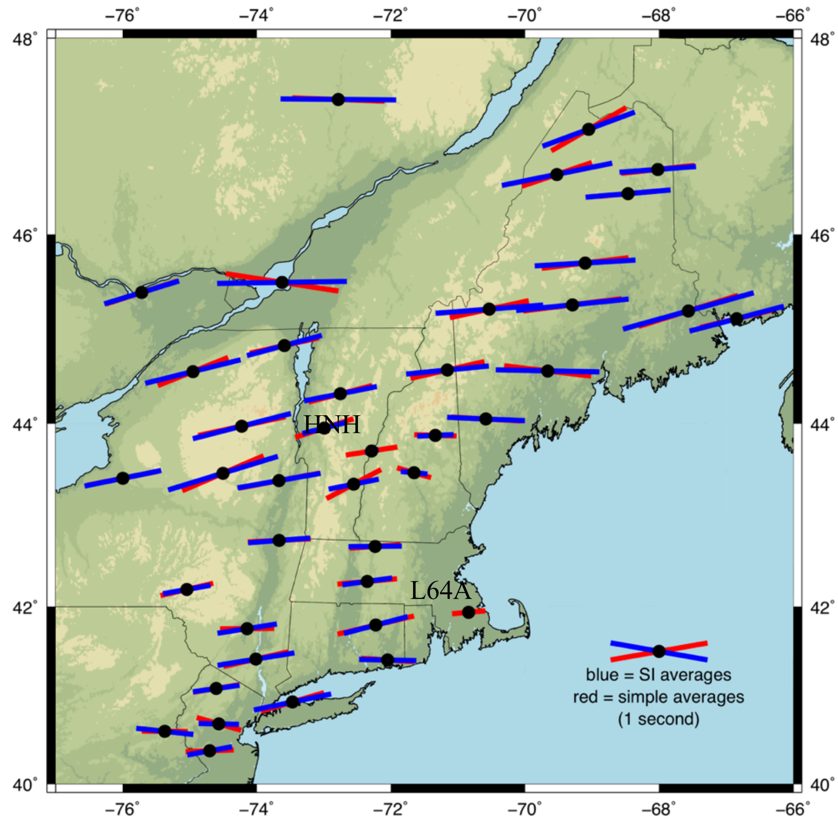

Figure 5: The station-averaged splitting parameters obtained by two different averaging methods; the blue bars indicate the values obtained by the SI method, and the red bars indicate the values obtained by simple averaging. The black dots indicate the location of 41 stations. The bars are scaled in proportion to the delay times and are oriented parallel to the estimated fast polarizations.

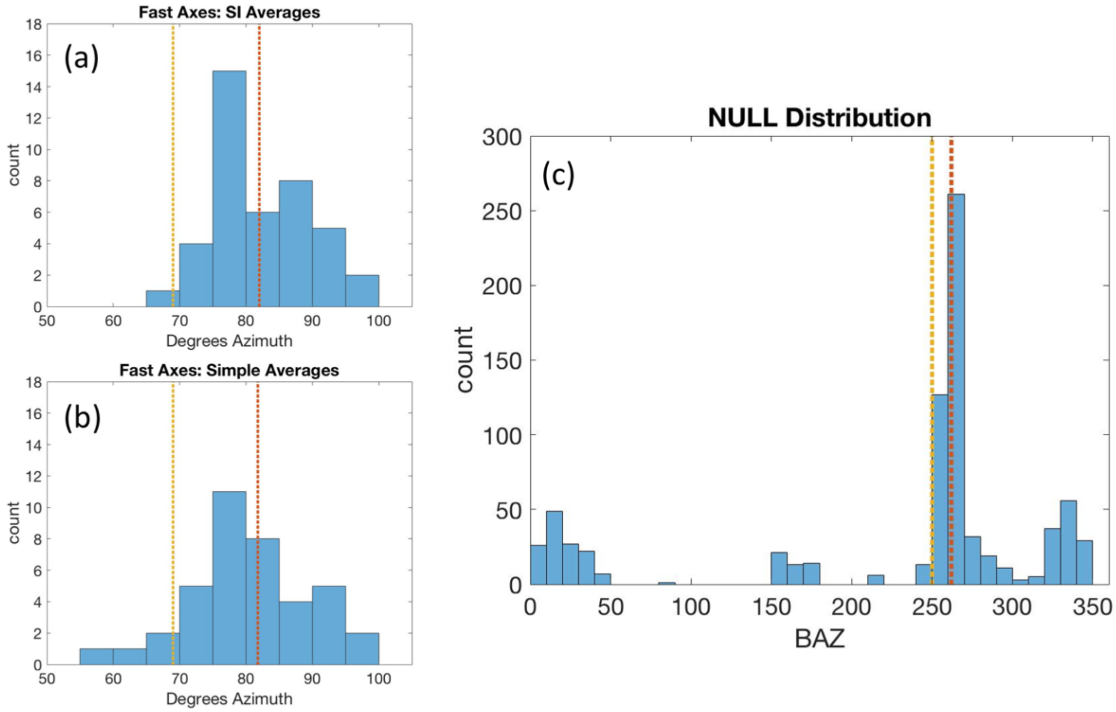

Figure 6: The distributions of averaged fast axes orientations and the back azimuths that yielded NULL measurements. The red dashed lines indicate the mean fast axes orientations, and the yellow dashed lines indicate the regional absolute plate motion obtained from HS3-NUVEL1 plate model. (a) shows the averages obtained using the SI technique (modulo 180°), (b) shows the averages obtained by simple averages of only the split measurements, and (c) shows the back azimuths that yielded the NULL measurements.

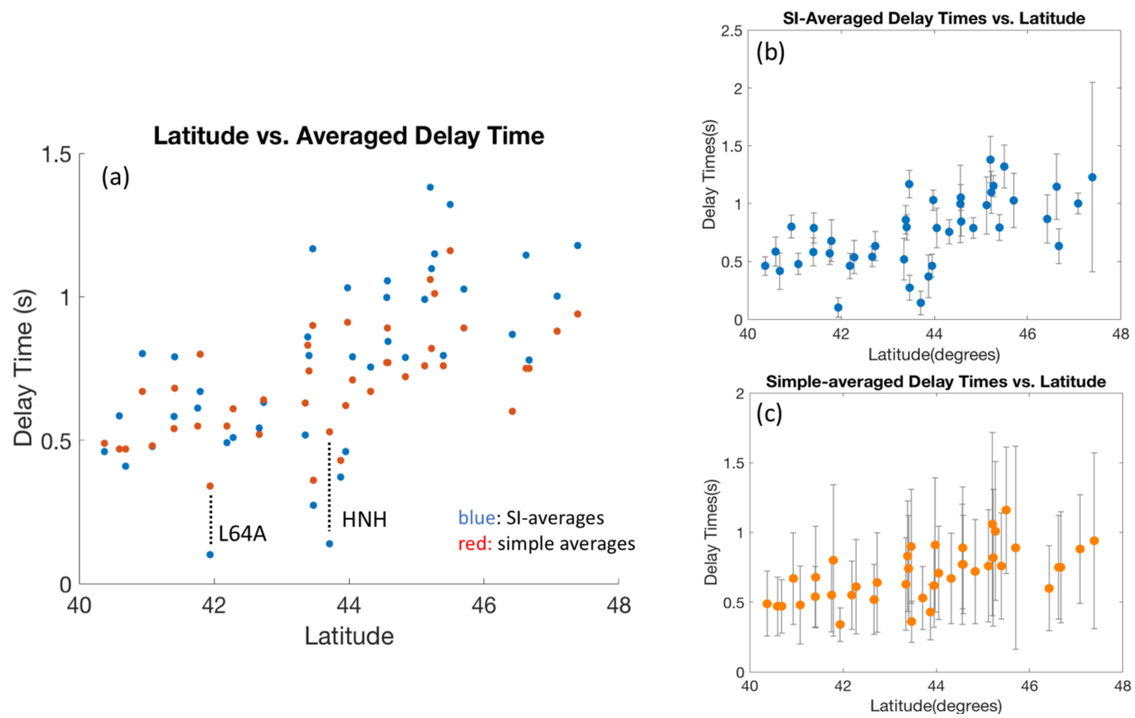

Figure 7: Regional trend of the delay times. (a) indicates the trends of averaged delay times plotted with respect to the latitude; the blue dots represent the values obtained by SI technique, and the red dots represent the values obtained by simple averaging. (b) and (c) each indicate individual trends of delay times with error bars.

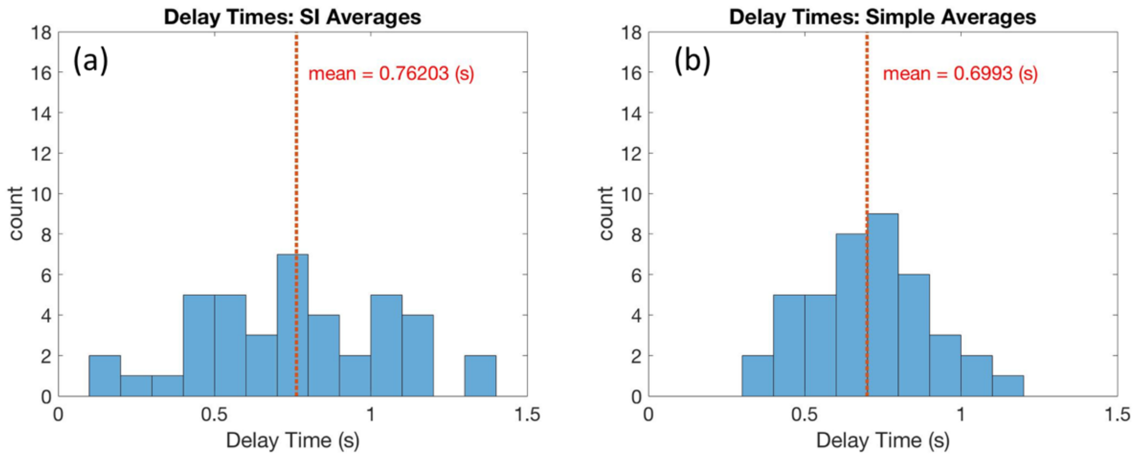

Figure 8: The distribution of station-averaged delay times obtained by both SI technique and simple averaging. The red dashed lines here indicate the mean delay times of each distributions. (a) indicates the delay times obtained by the splitting intensity technique, (b) indicates the delay times obtained by simple averages.

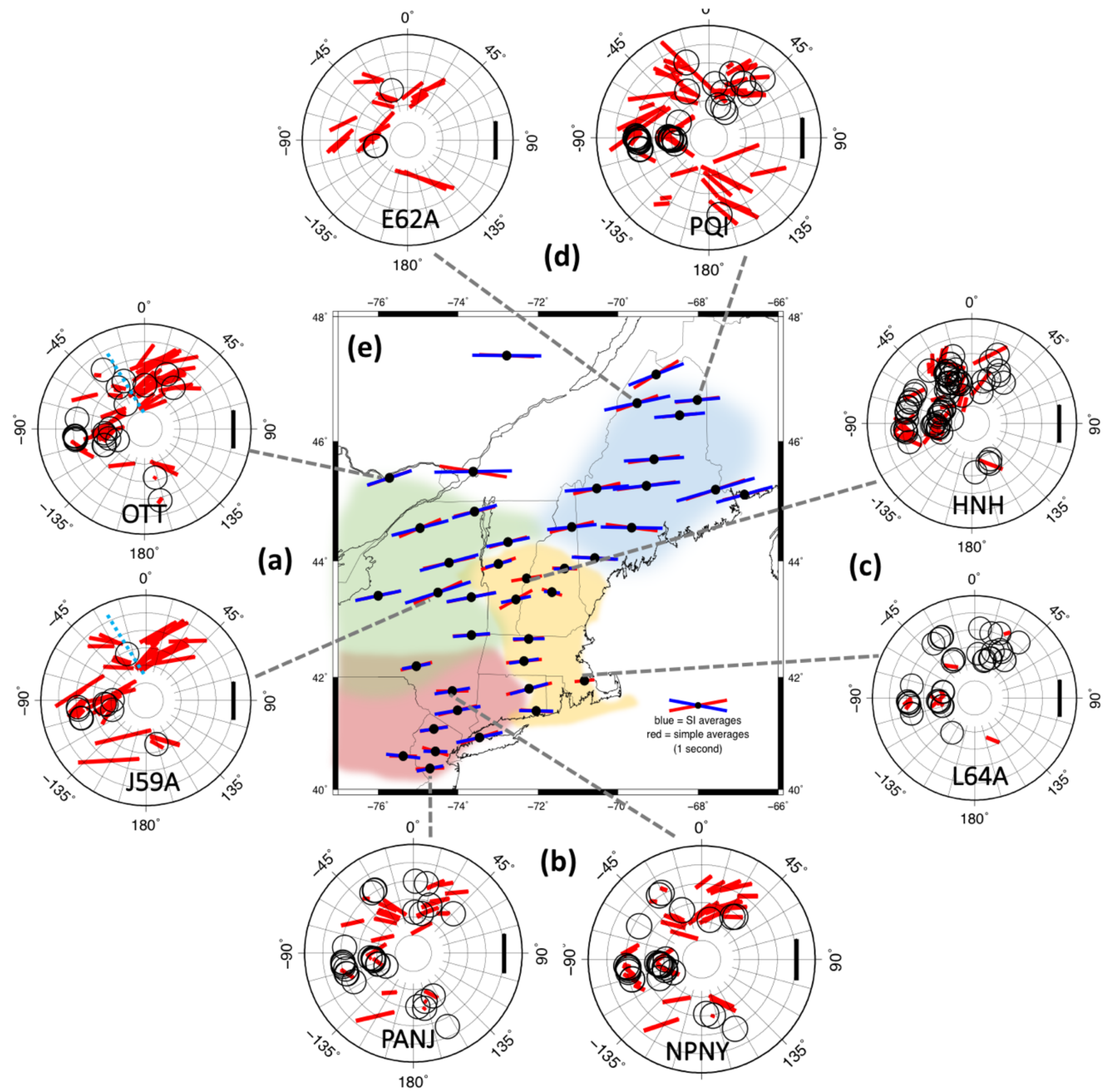

Figure 9: The four anisotropic domains grouped based on similar patterns of back azimuthal dependence, plotted with representative examples of stereonet plots from each domain. The example stereonet plots are representative of (a) green domain, (b) red domain, (c) yellow domain, and (d) blue domain, respectively. The blue dashed lines in (a) for stations OTT and J59A mark the back azimuth at which the delay times drastically drop from the northeast to the northwest. The stereonet (d) and (e) are representative of yellow domain. The plots (a) – (d) follow the convention described in Figure 3c. The distances from the center of the stereonet represent inclination angles. Beginning with the inclination angles of 0 degrees at the center, the angle increases 3 degrees with each ring, reaching inclination angle of 18 degrees at the rim. (e) indicates the spatial distribution of the four domains, plotted with the pairs of averaged splitting parameters displayed in Figure 5.

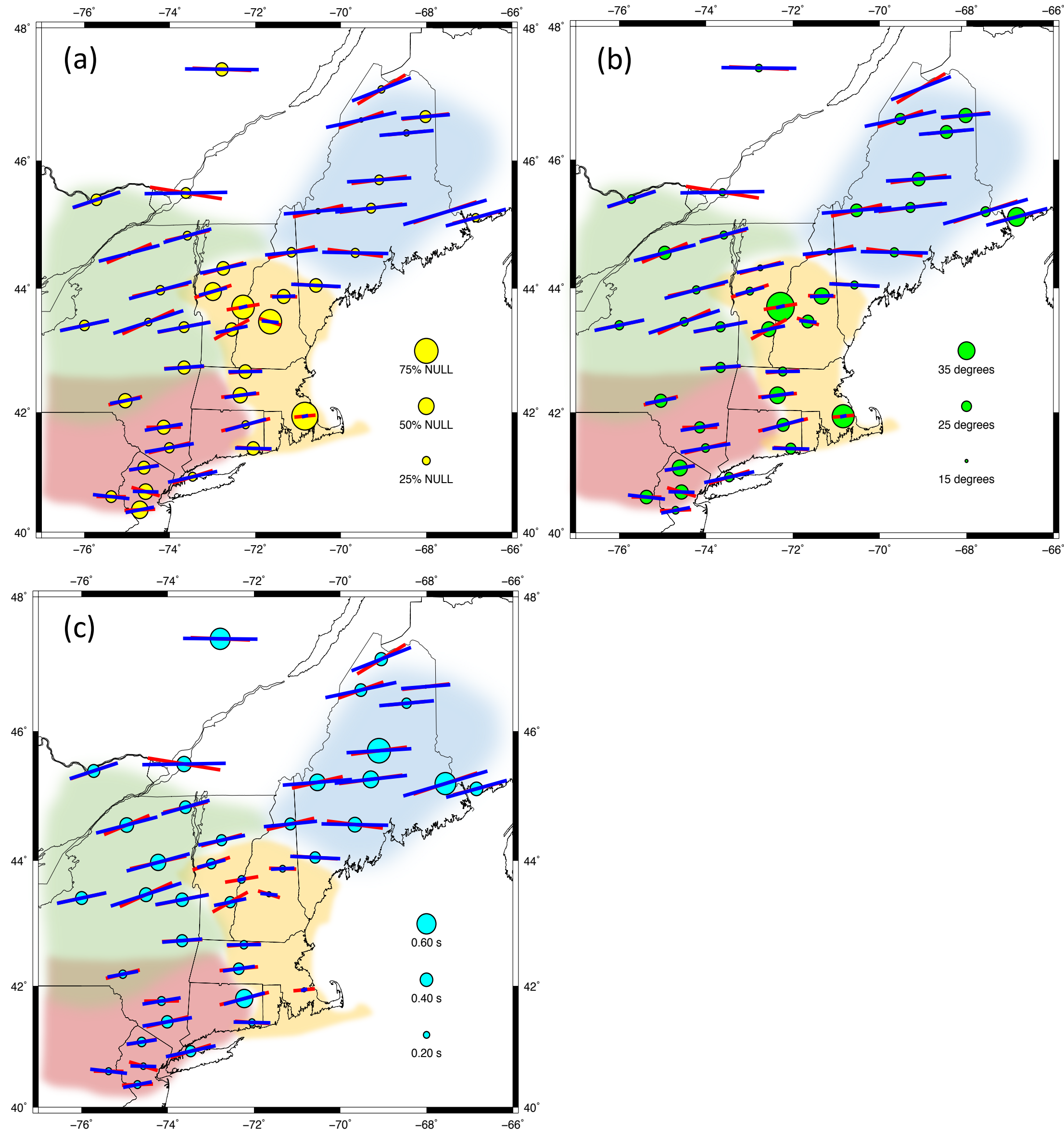

Figure 10: The regional distributions of selected statistic traits. (a) exhibits the proportion of NULL measurements within the individual station datasets, (b) exhibits the standard deviation of fast axes orientations, and (c) exhibits the standard deviation of delay times, as measures for the degree to which the both splitting parameters fluctuate.

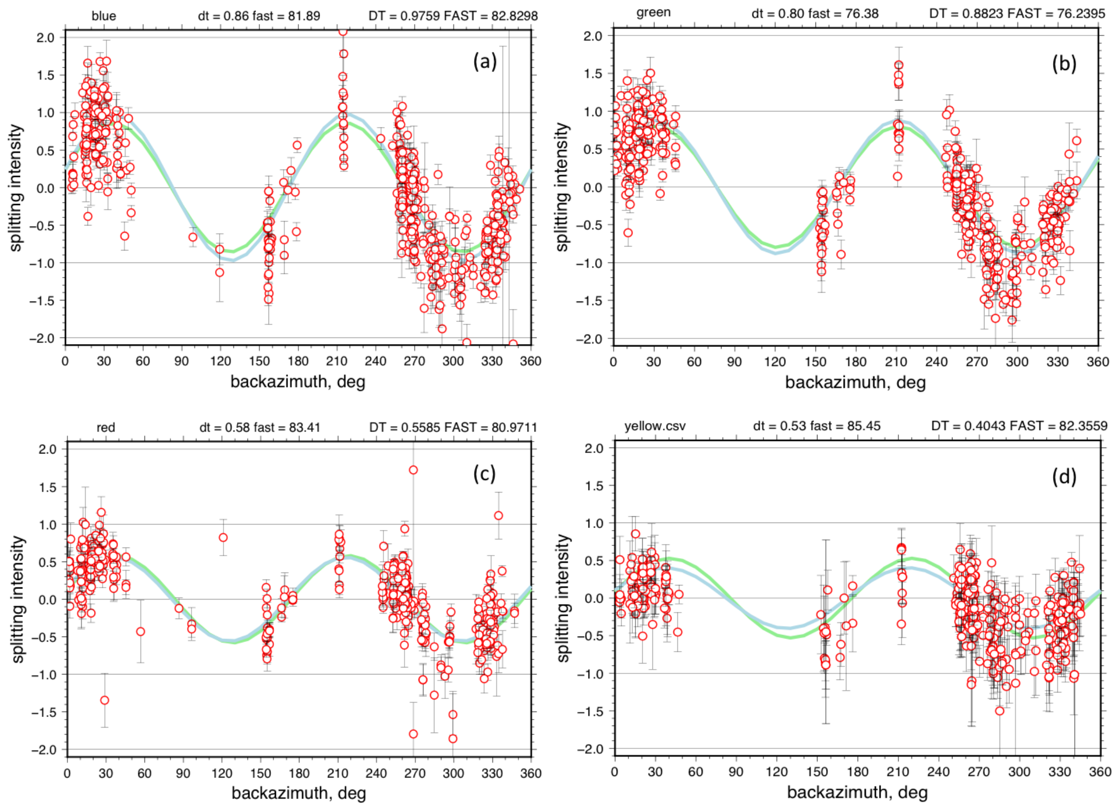

Figure 11: The sinusoid pattern of splitting intensity values fitted to all measurements within each domain. The blue lines in the SI plots are the best-fit curves determined by a least-squares fit for the parameters of function, $\delta t \times \sin[2(\varphi_o - \varphi)]$. The green lines are curves predicted based on the mean fast axis and delay time of all split measurements within the specific domain. (a) indicates the blue domain, (b) indicates the green domain, (c) indicates the red domain, and (d) indicates the yellow domain.

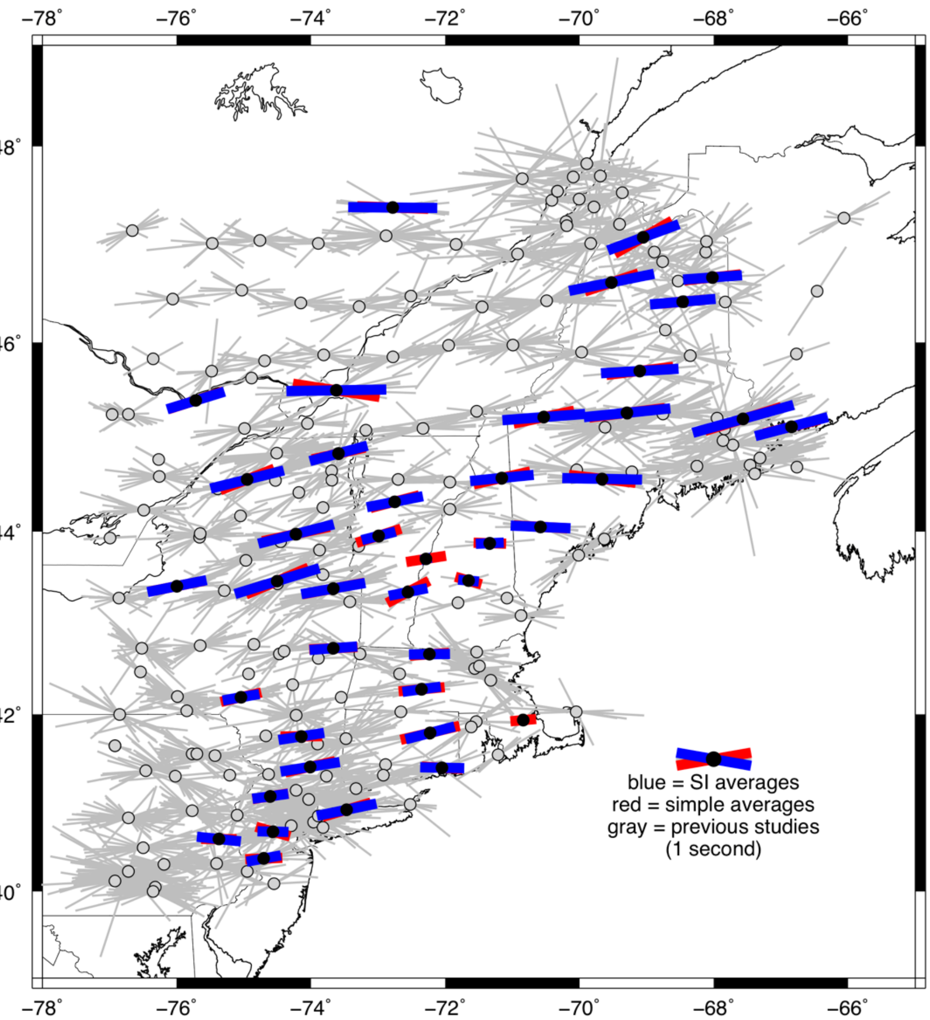

Figure 12: Comparison of our results with those measured by the previous studies done in the region. The gray bars indicate both the single-event and station-averaged splitting parameters reported by the previous studies. The blue and red bars indicate our station-averaged splitting parameters, quantified by SI technique and simple-averaging, respectively. All bars are aligned to the orientations of fast polarization and are scaled proportional to the delay times.

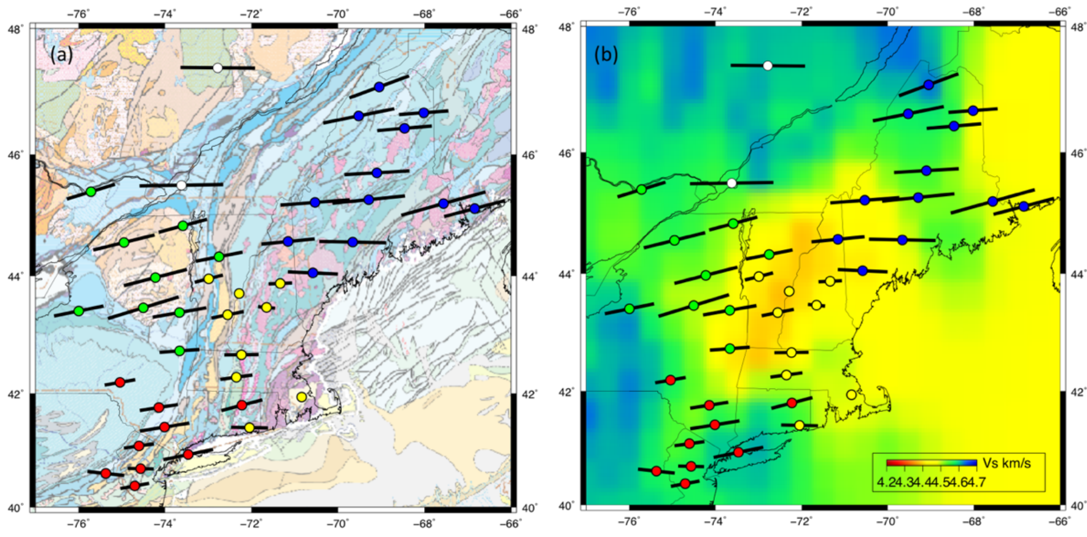

Figure 13: The comparison of anisotropic domains with (a) the surface geological map based on Reed et al. (2005) and (b) the shear wave velocity distribution of Shen & Ritzwoller (2016) at 90km depth. The four anisotropic domains are indicated by the different colors of the circles plotted at the location of each station. The white stations are stations LATQ and MNTQ, which were deemed sufficiently different from the green and blue domains but were not sufficient to form a domain, due to the lack of station and sparsity. The black bars indicate the splitting parameters obtained by the SI technique.

Appendices

Figures A1 – A33: Datasets Used for Comparison Between Stations. Each figure consists of (a) the stereo plots showing the individual splitting parameters measured using the Rotation-Correlation method, (b) the comparison between the predicted and the best-fit SI curves, (c) the histogram distribution of the individual fast polarization, and (d) the histogram distribution of the individual delay times. (a) and (b) follows the same plotting convention as described in the main text. The red dashed lines in (c) and (d) indicate the position of mean.

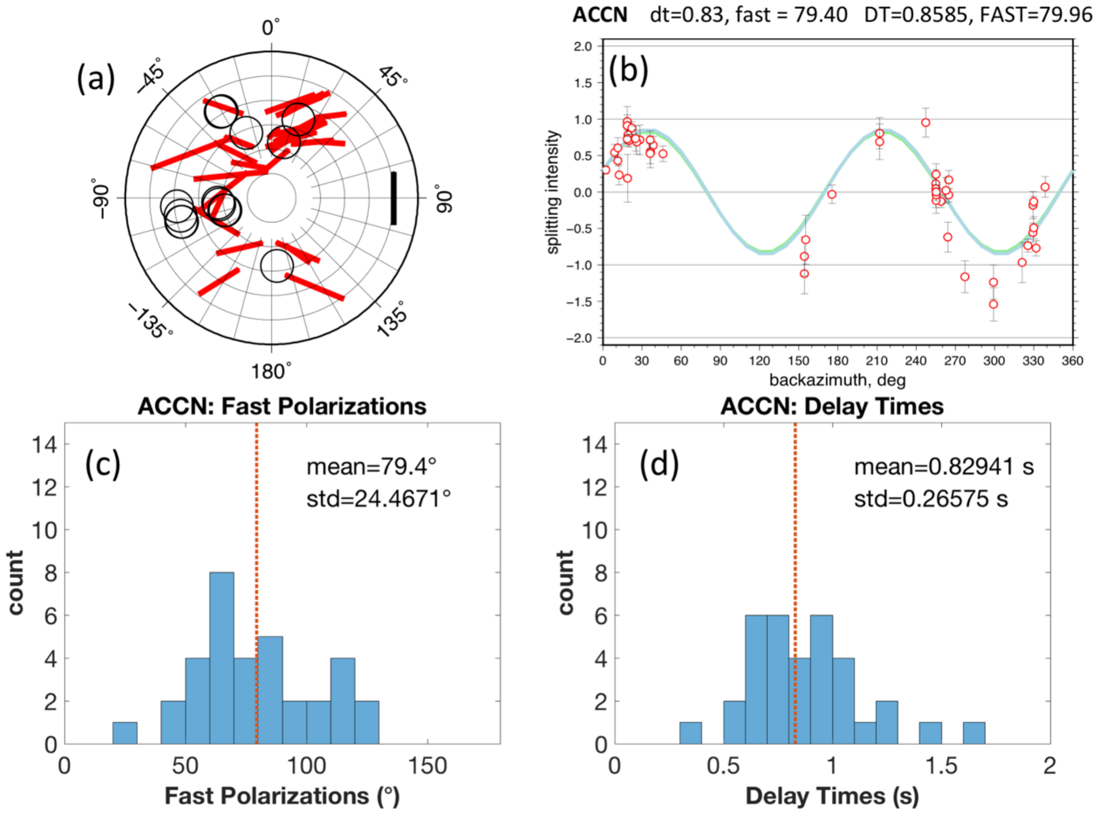

Figure A1: Station ACCN

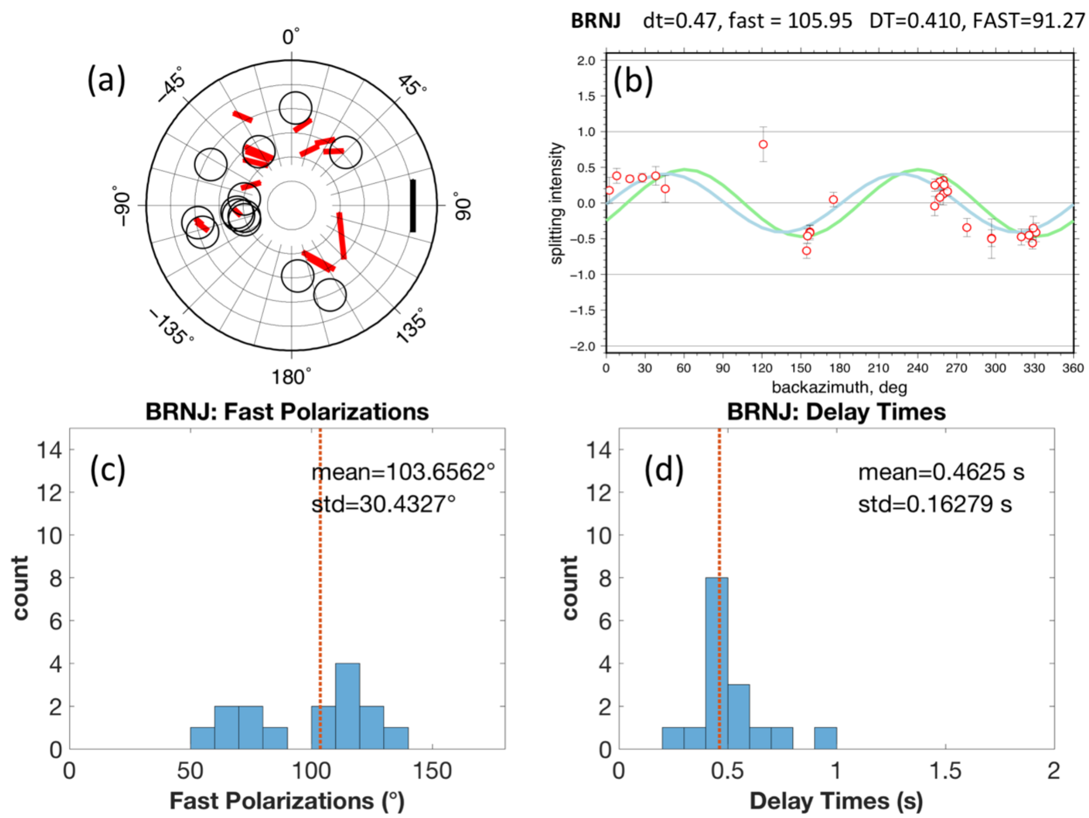

Figure A2: Station BRNJ

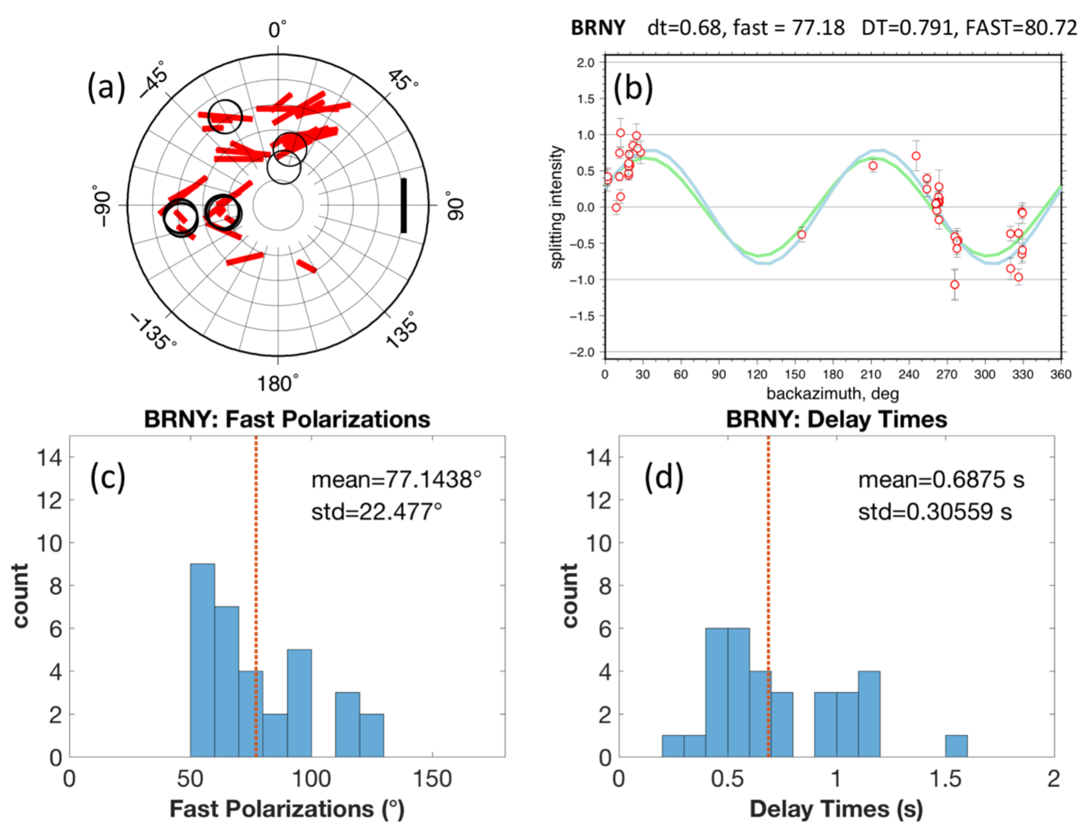

Figure A3: Station BRNY

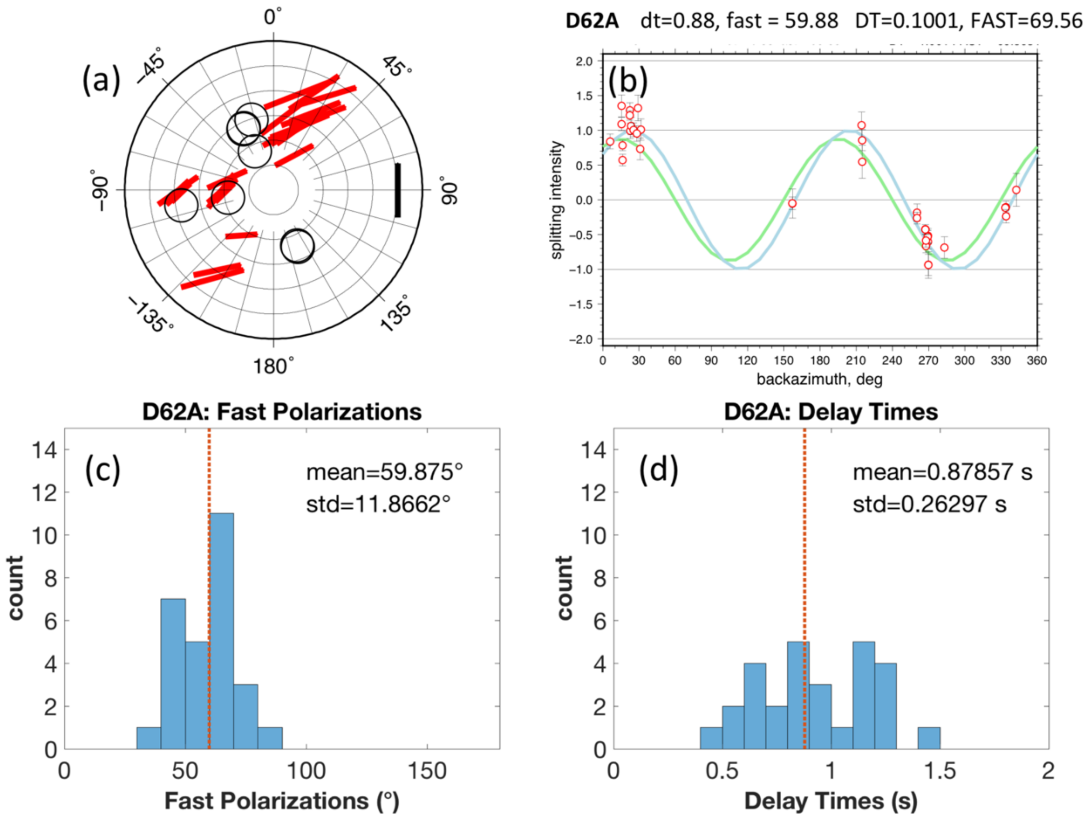

Figure A4: Station D62A

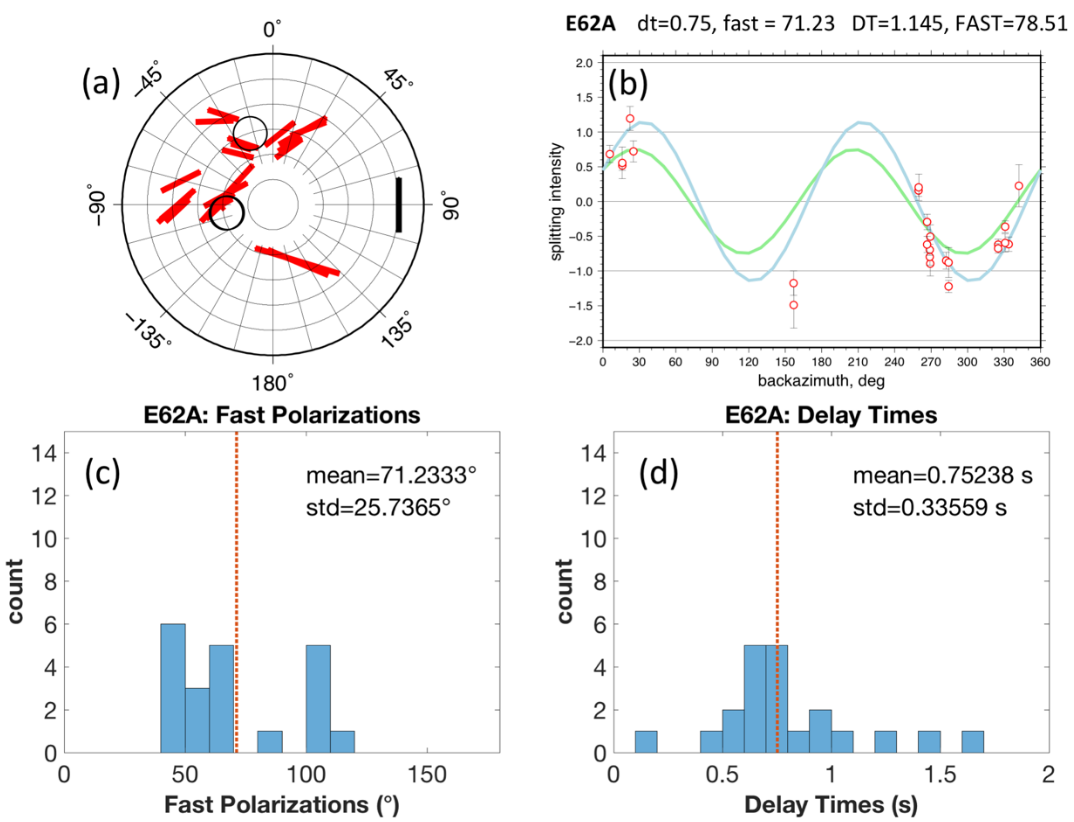

Figure A5: Station E62A

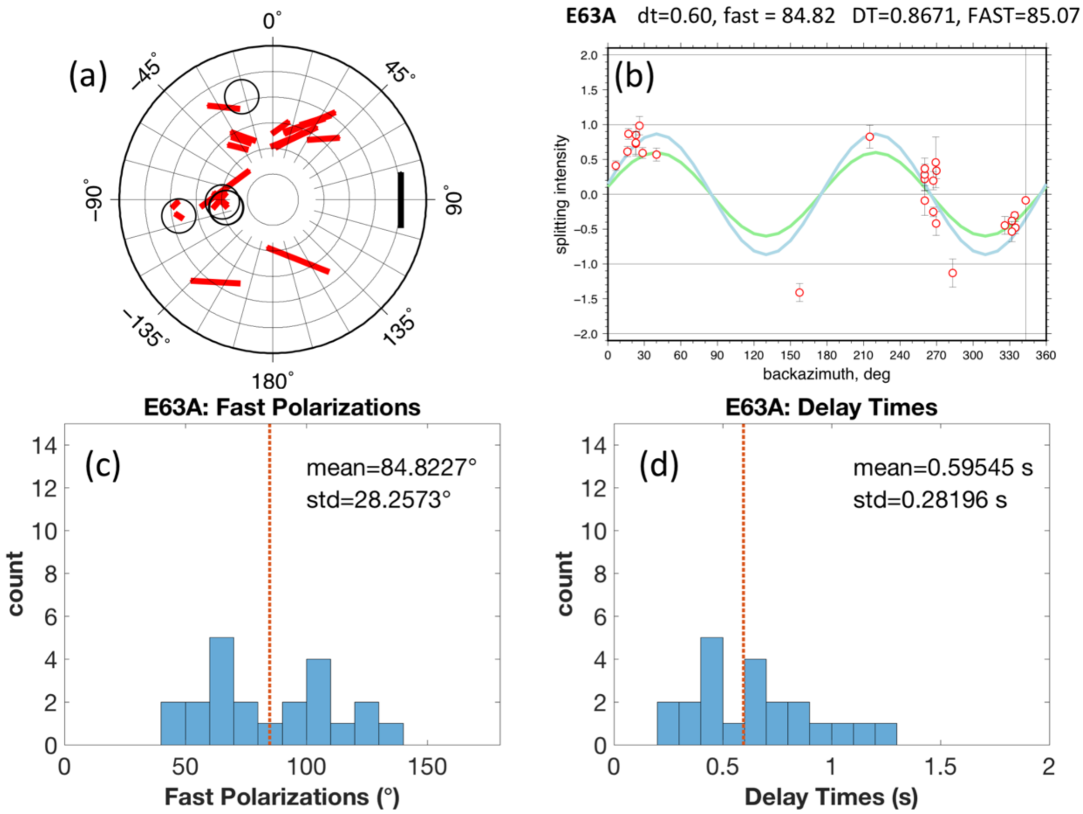

Figure A6: Station E63A

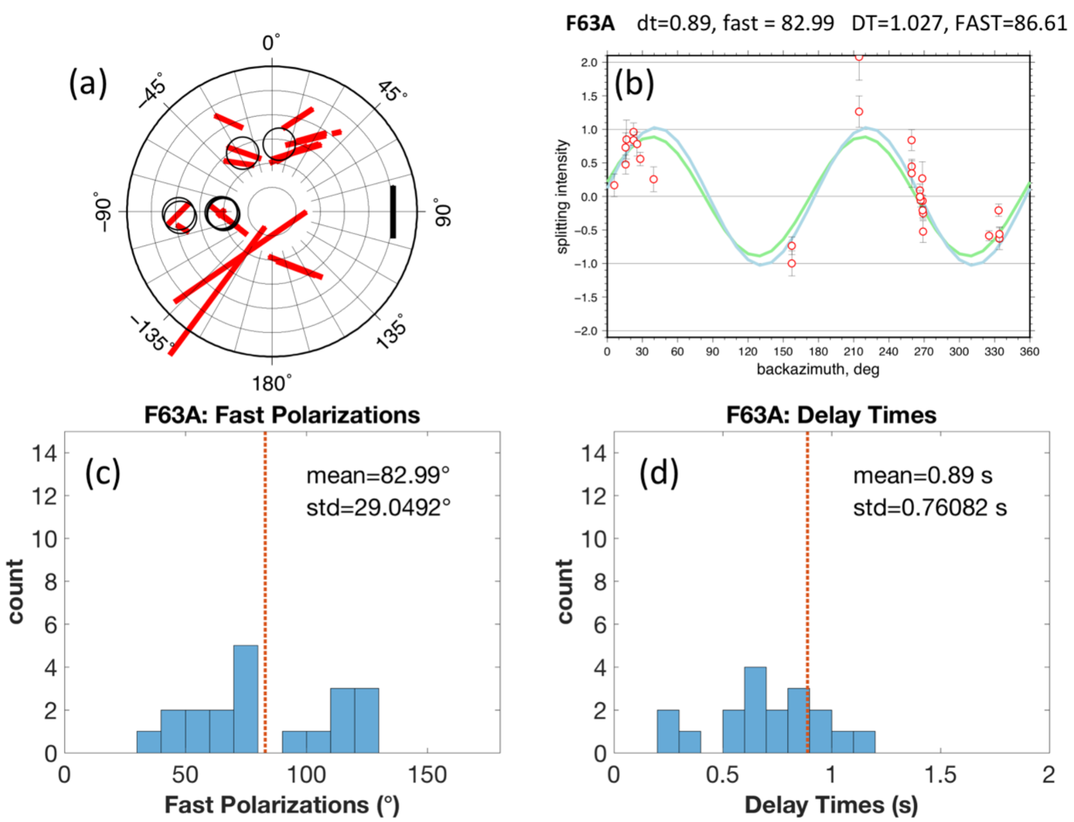

Figure A7: Station F63A

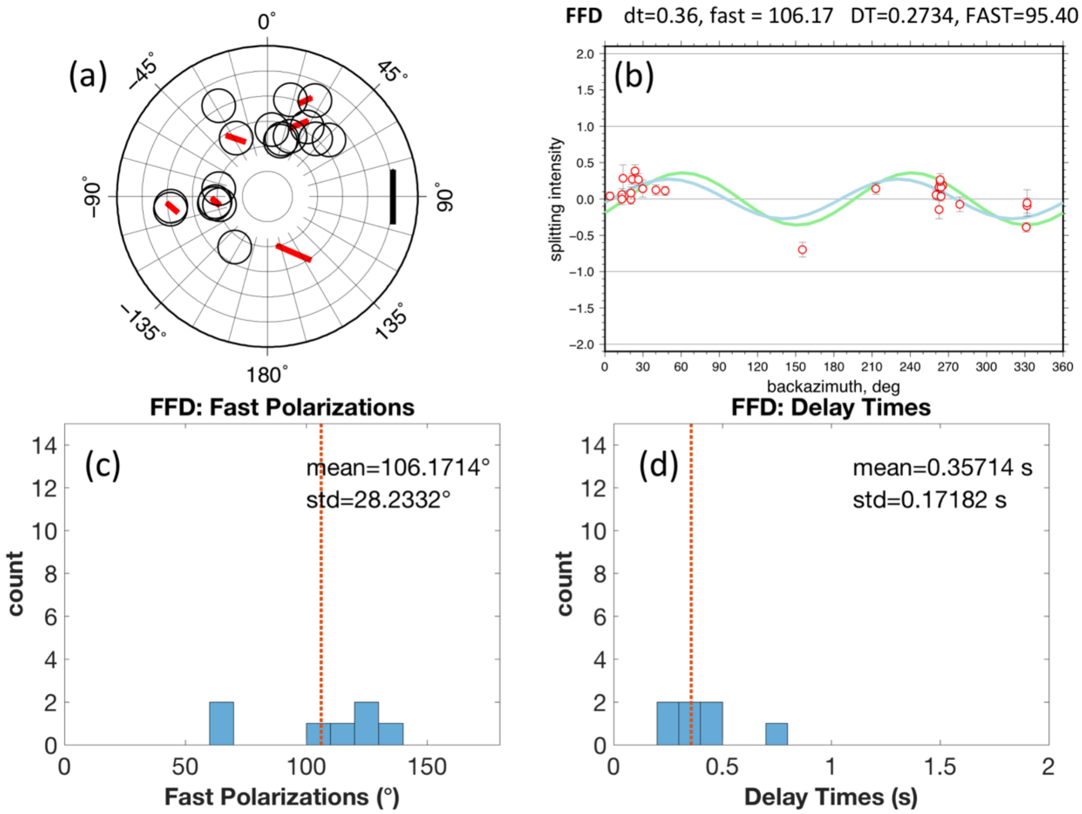

Figure A8: Station FFD

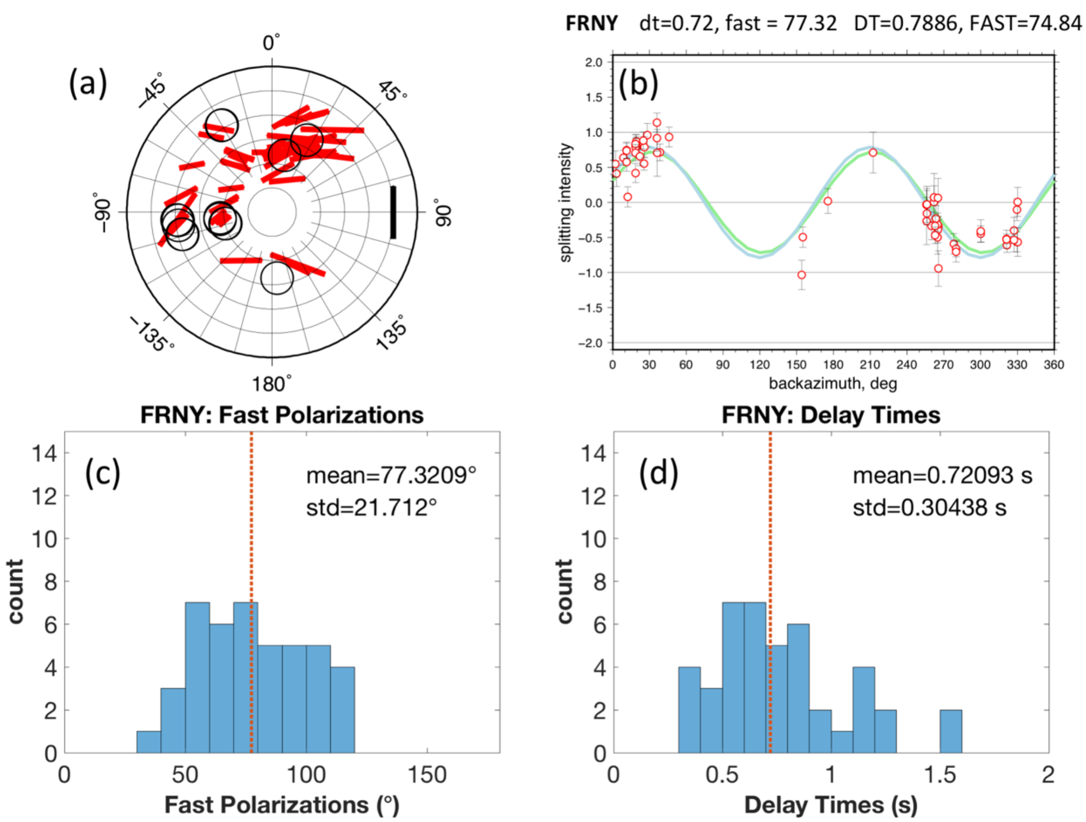

Figure A9: Station FRNY

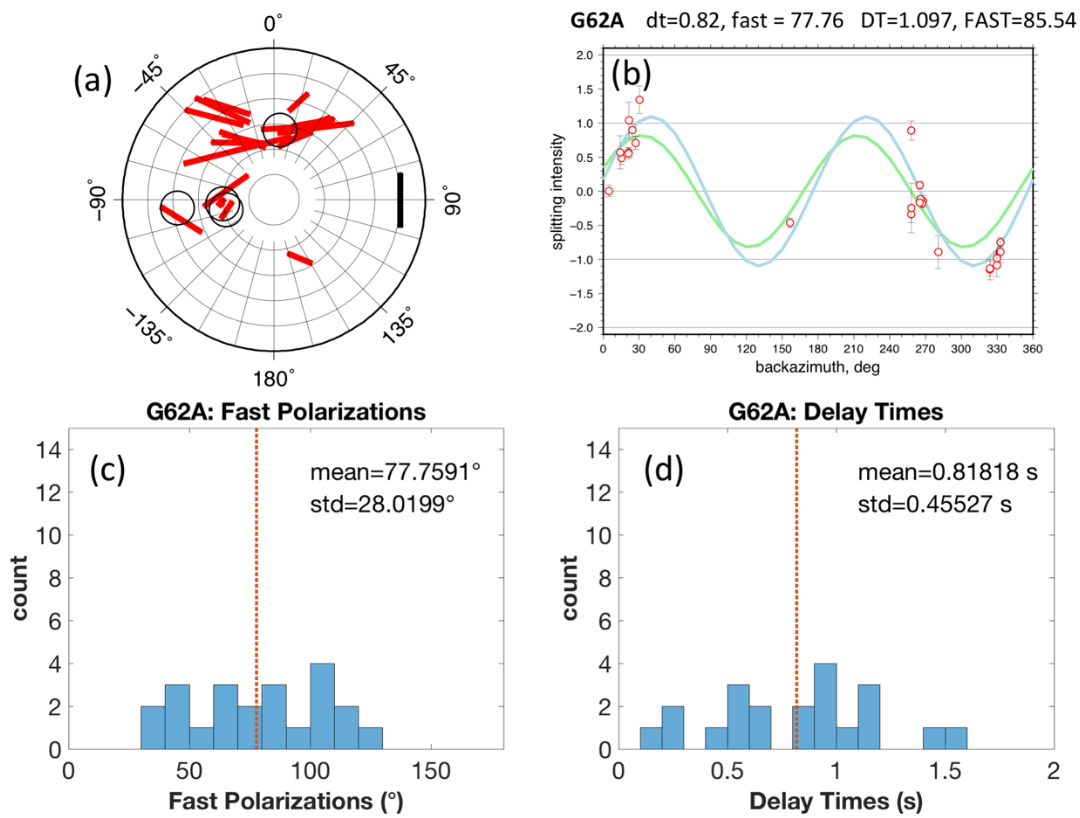

Figure A10: Station G62A

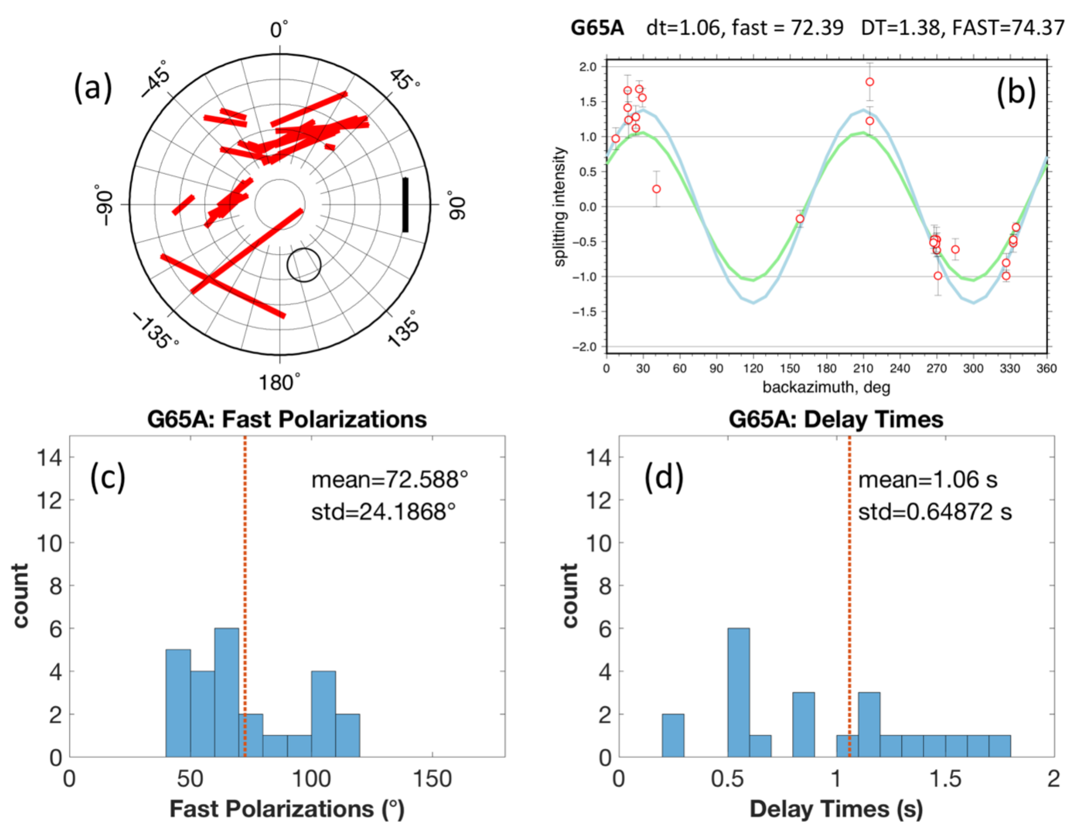

Figure A11: Station G65A

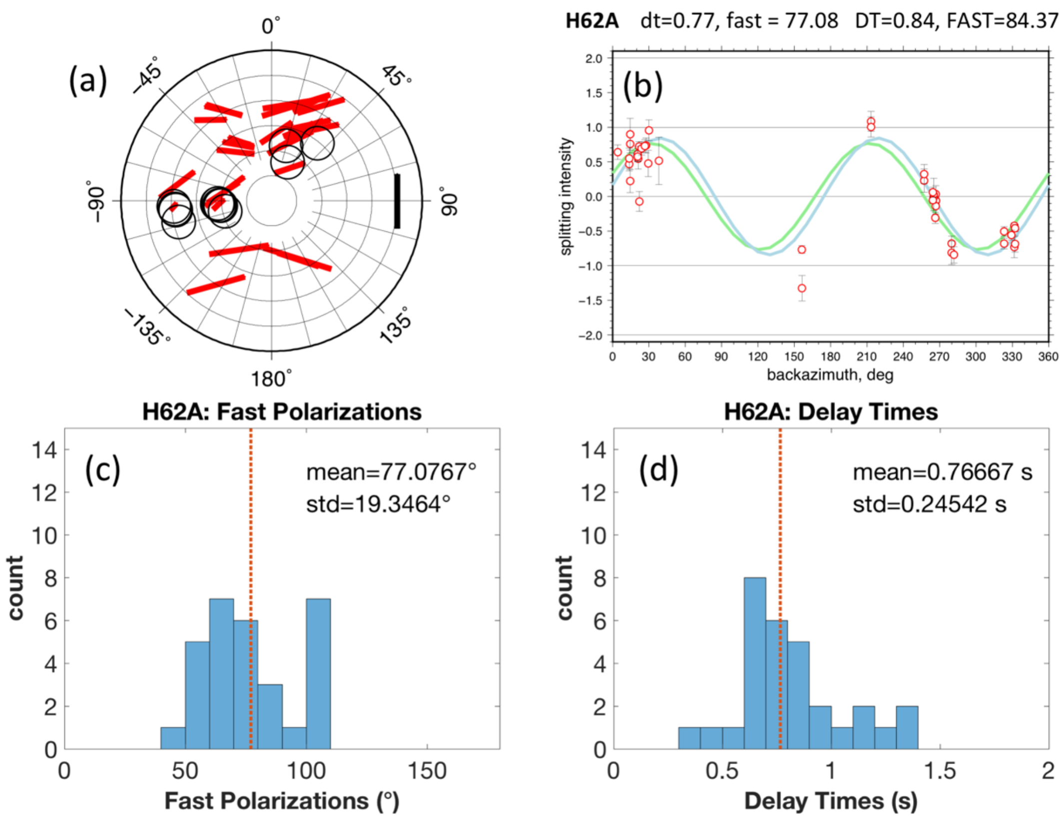

Figure A12: Station H62A

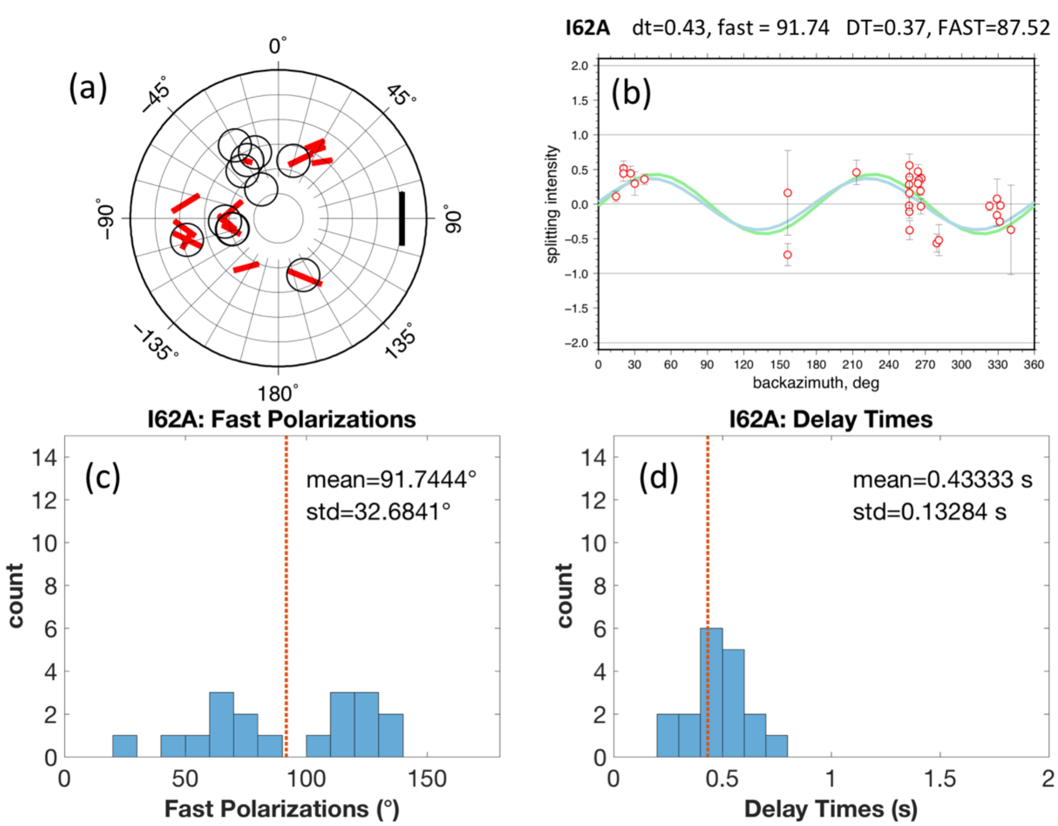

Figure A13: Station I62A

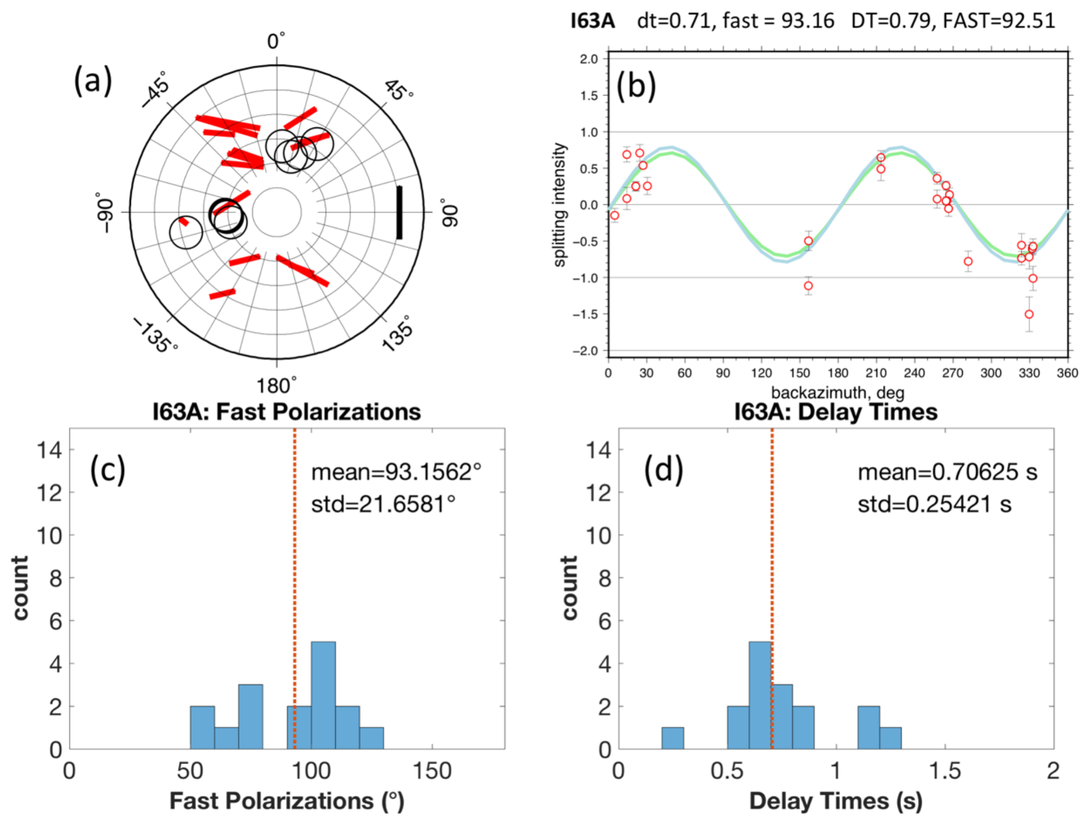

Figure A14: Station I63A

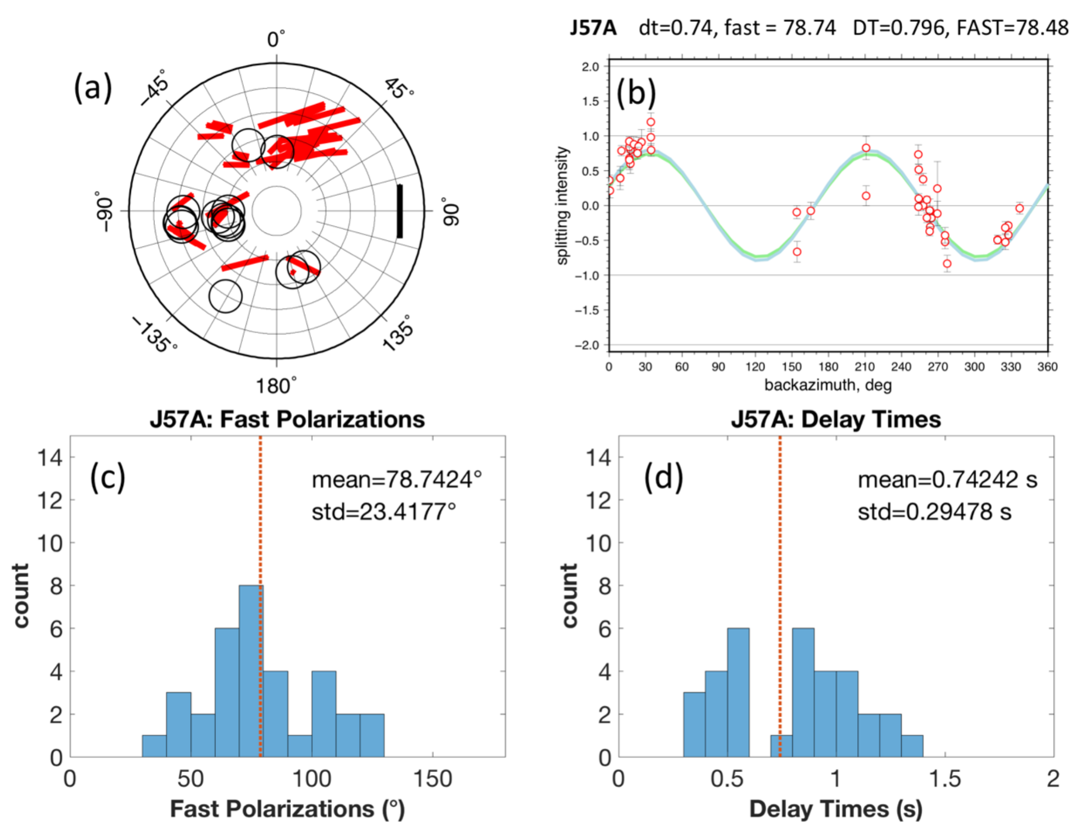

Figure A15: Station J57A

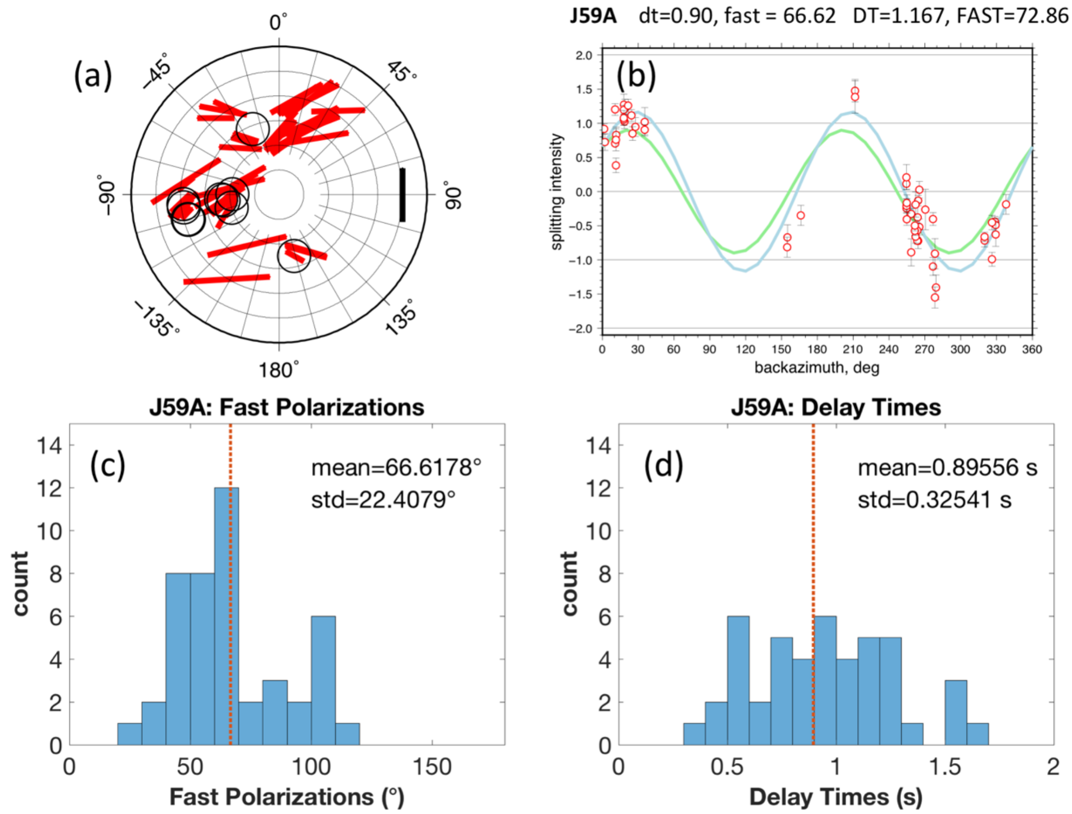

Figure A16: Station J59A

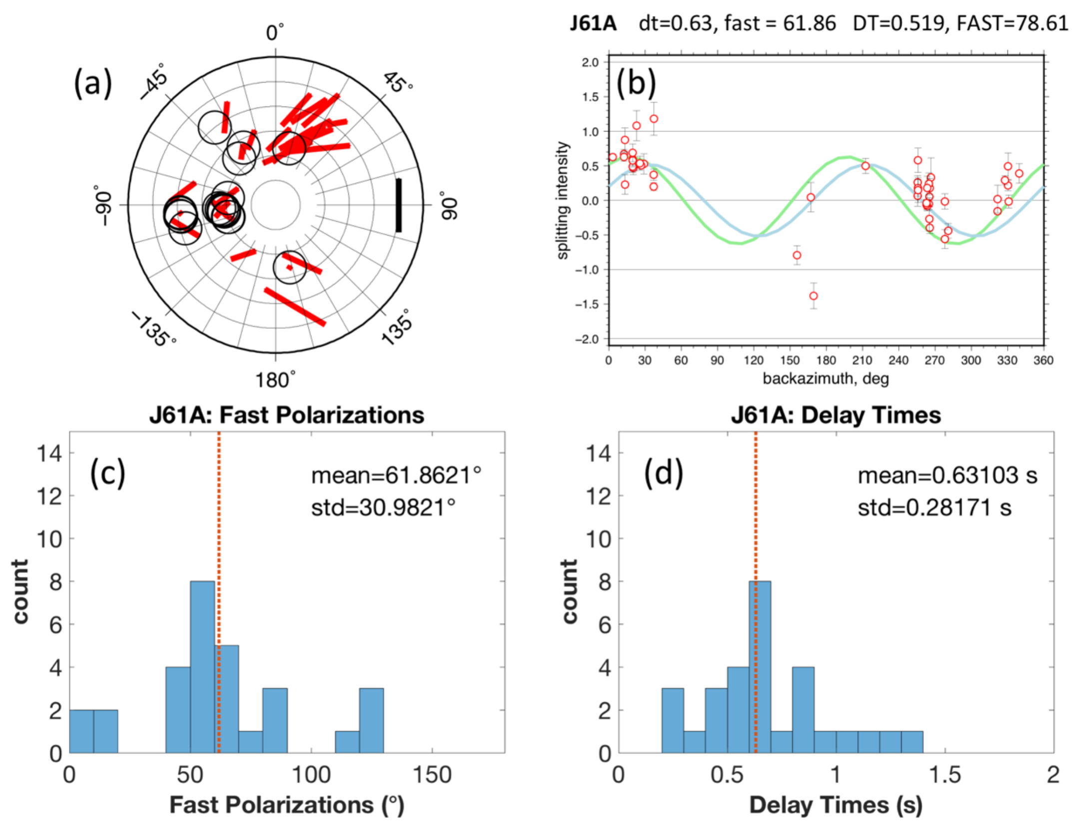

Figure A17: Station J61A

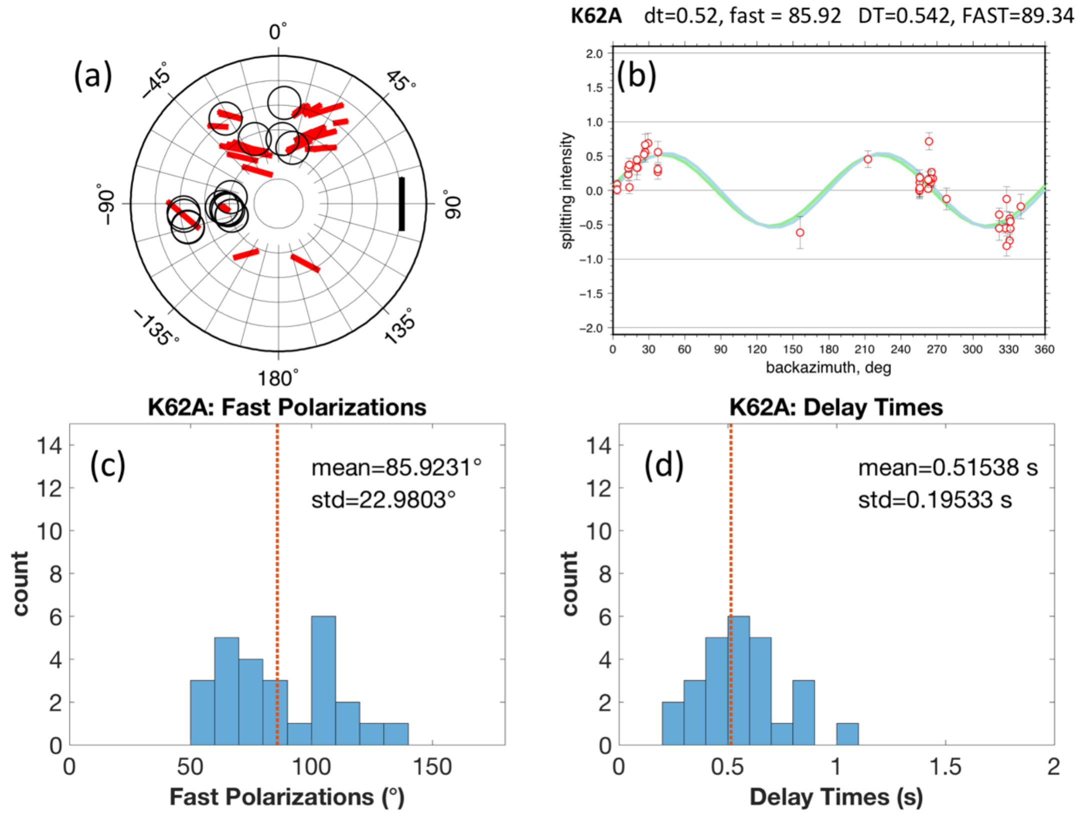

Figure A18: Station K62A

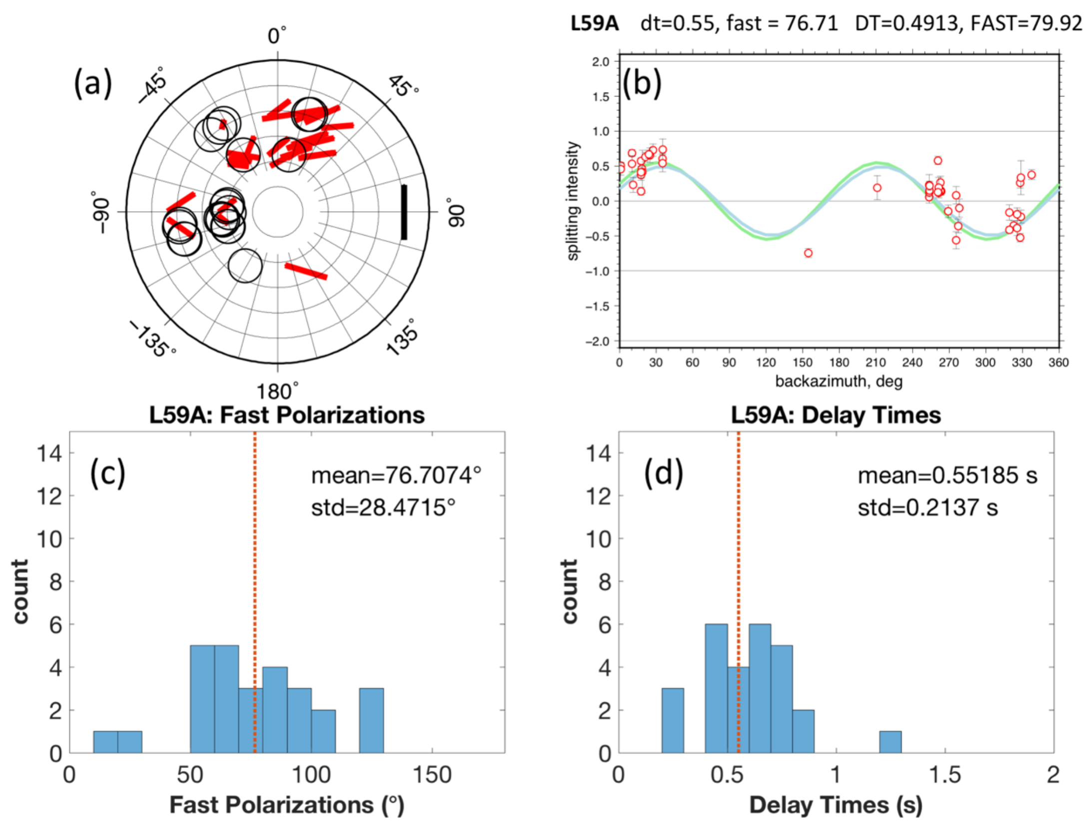

Figure A19: Station L59A

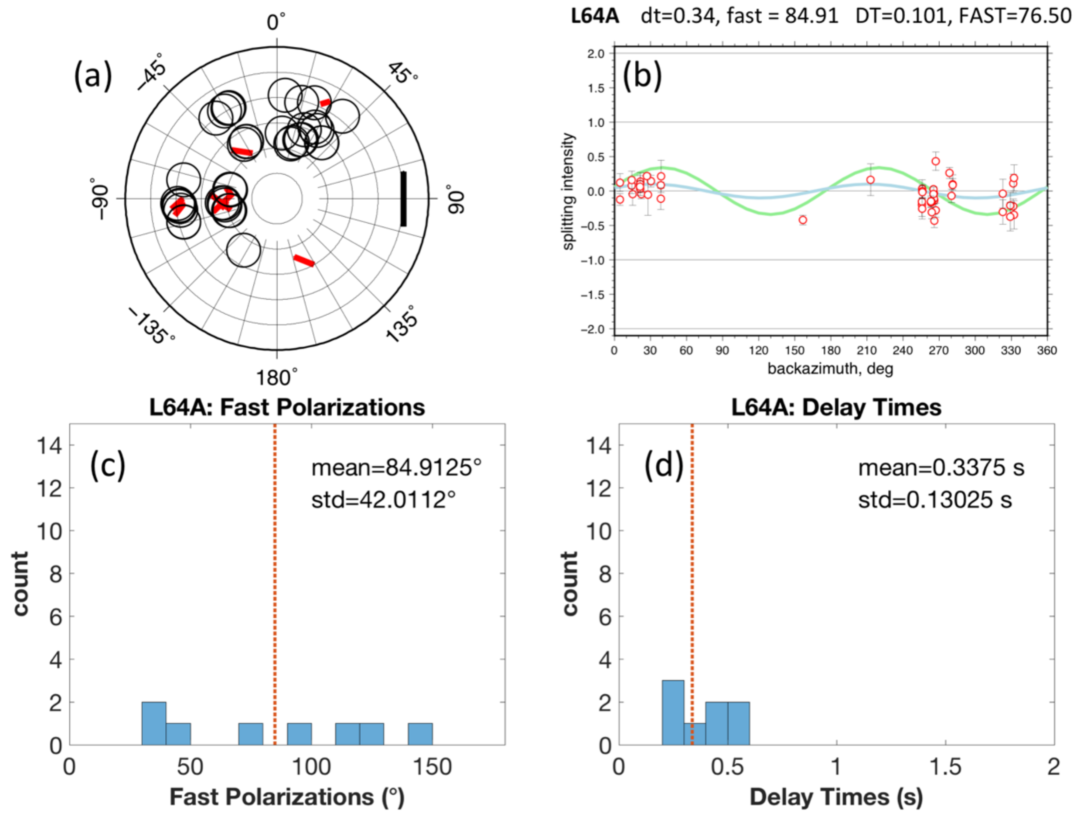

Figure A20: Station L64A

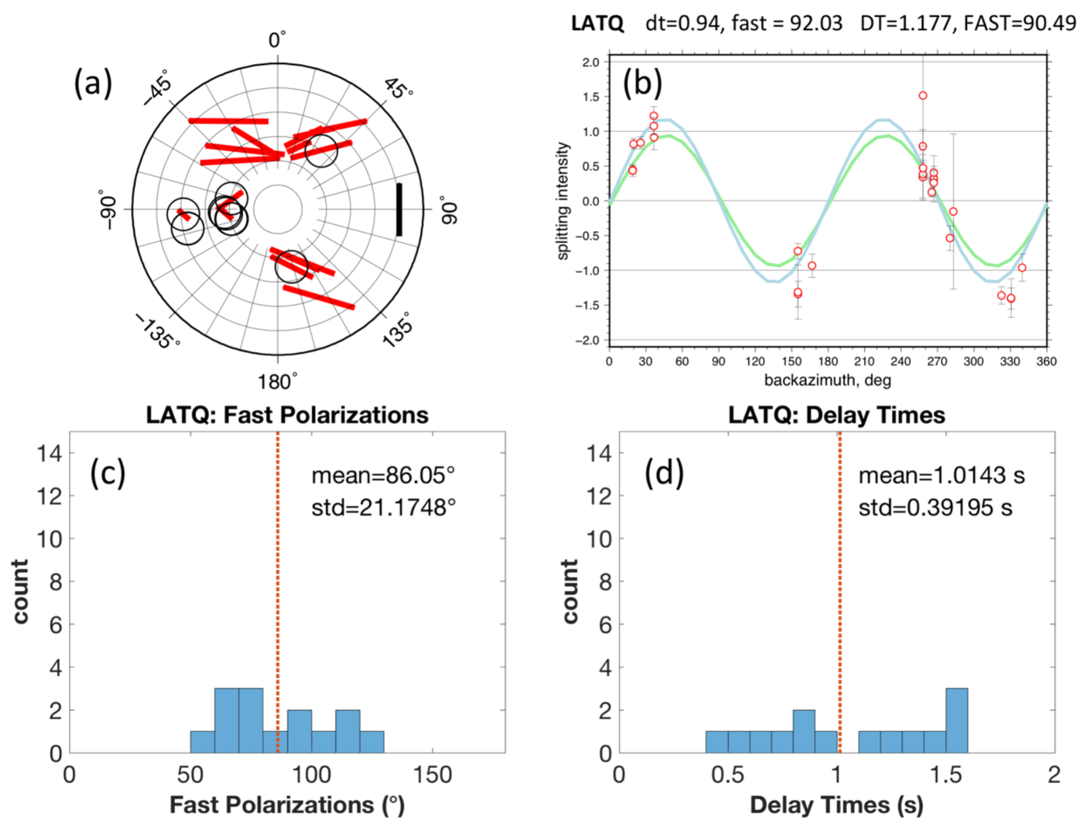

Figure A21: Station LATQ

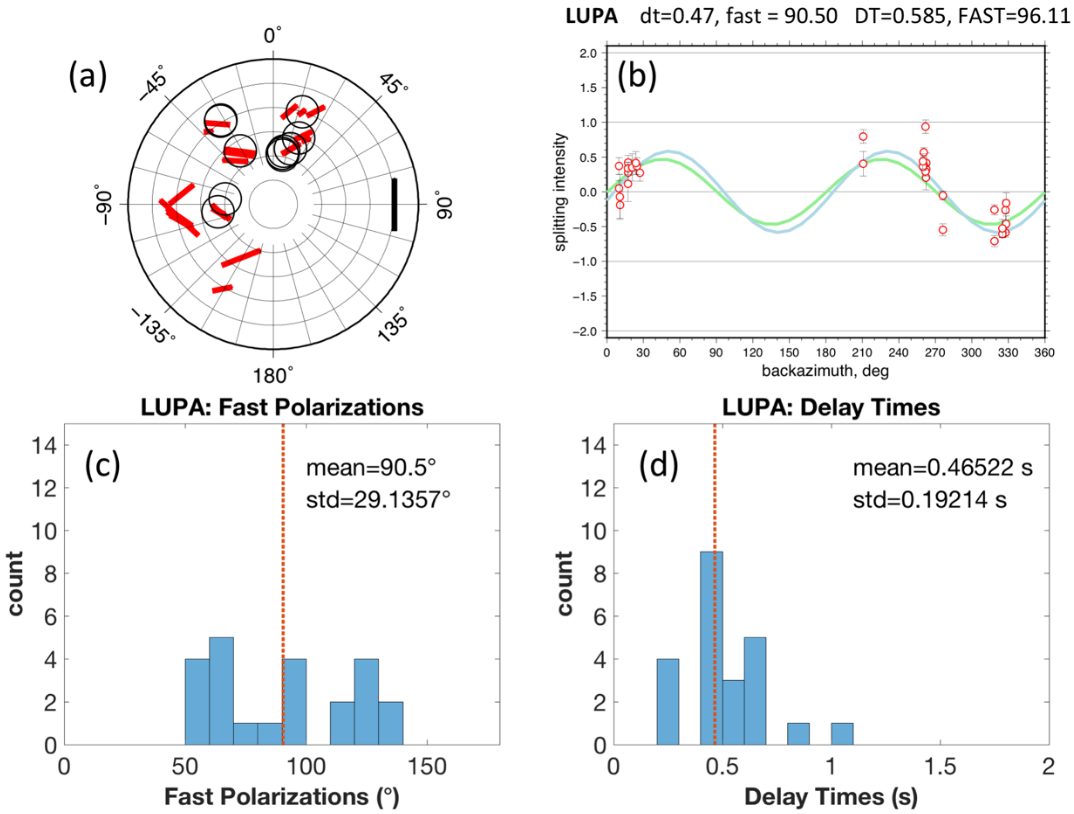

Figure A22: Station LUPA

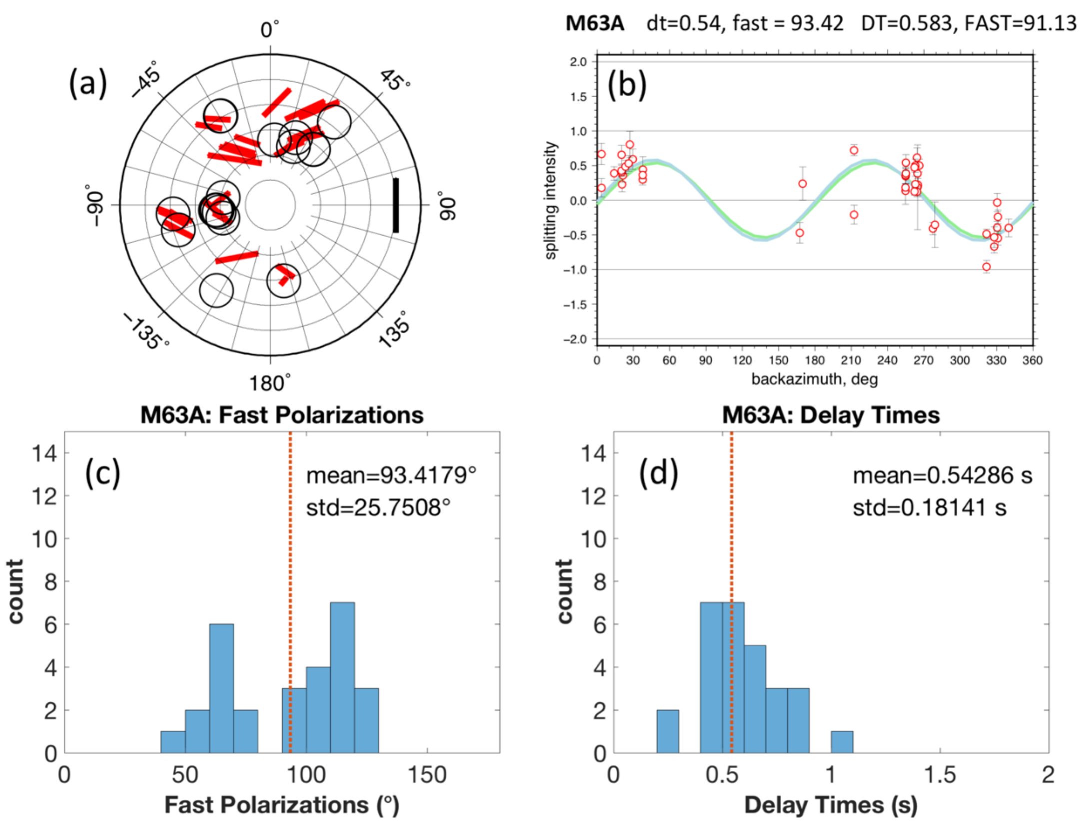

Figure A23: Station M63A

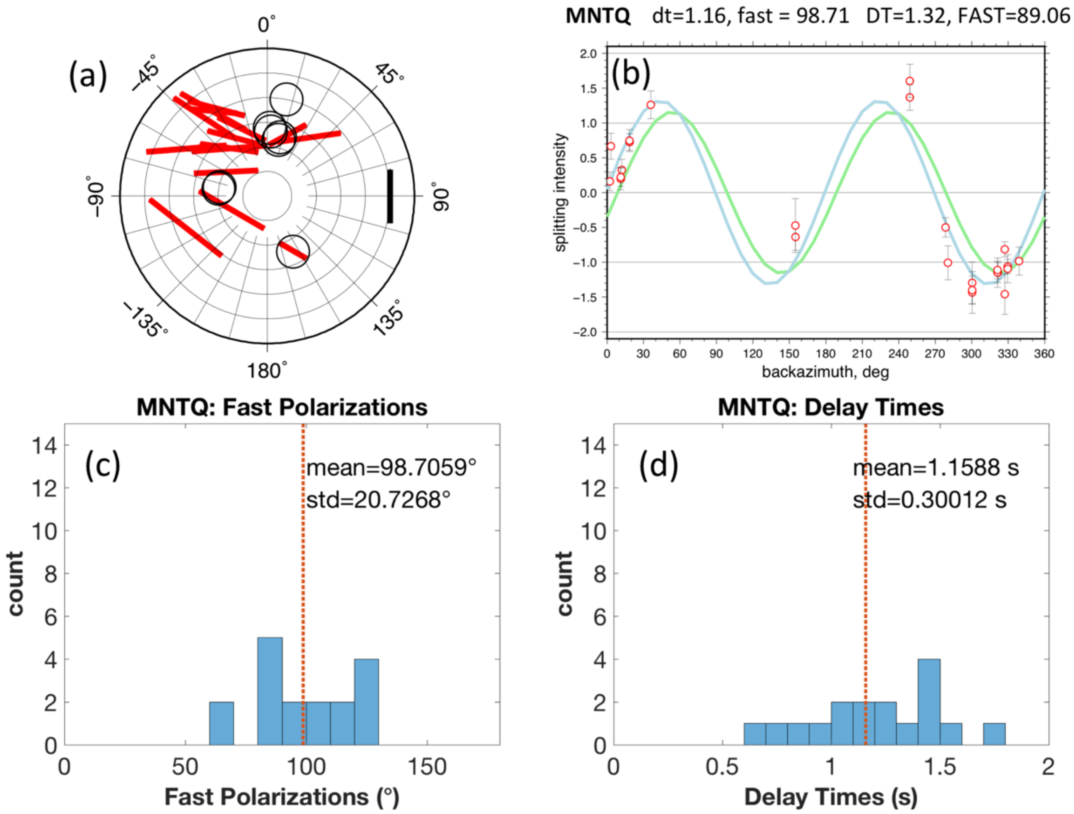

Figure A24: Station MNTQ

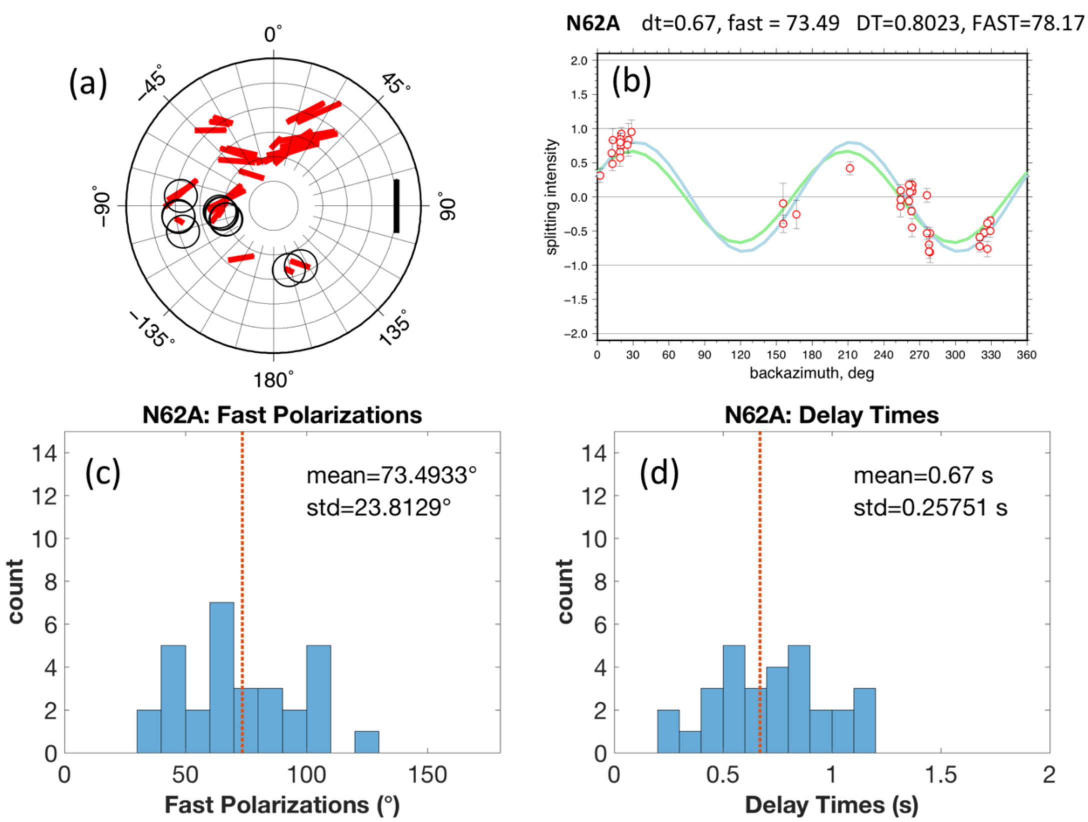

Figure A25: Station N62A

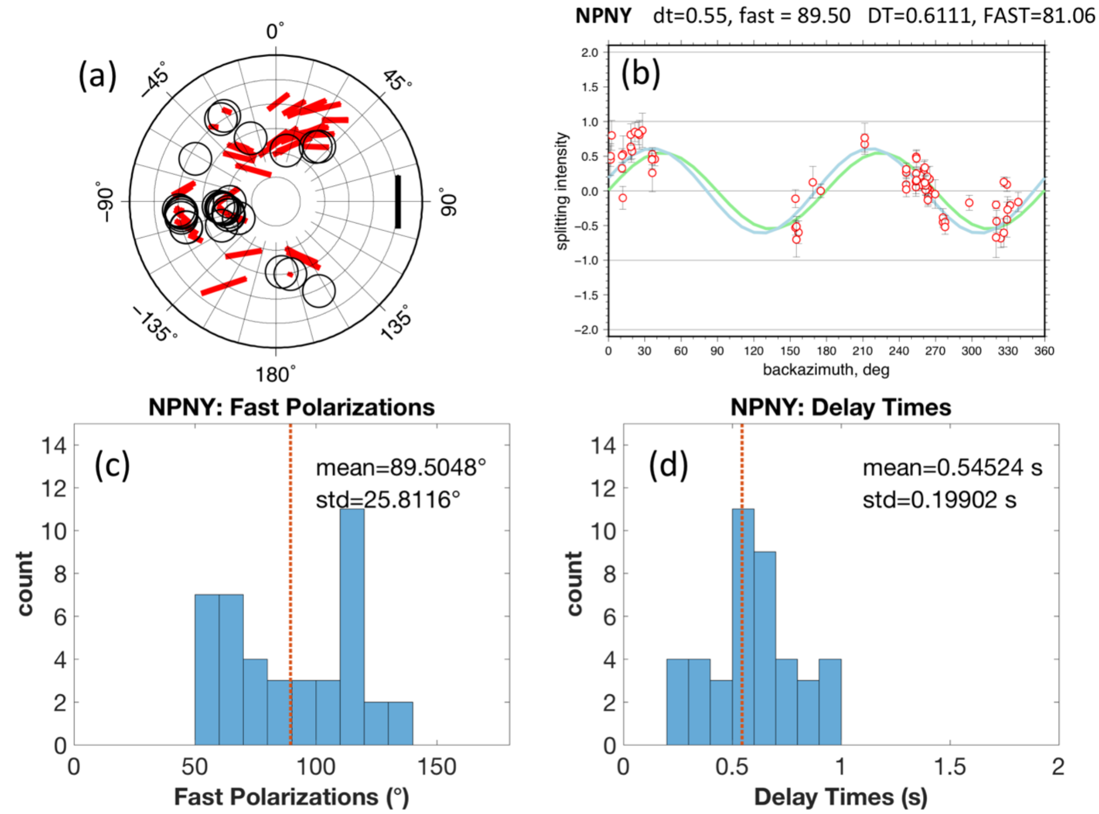

Figure A26: Station NPNY

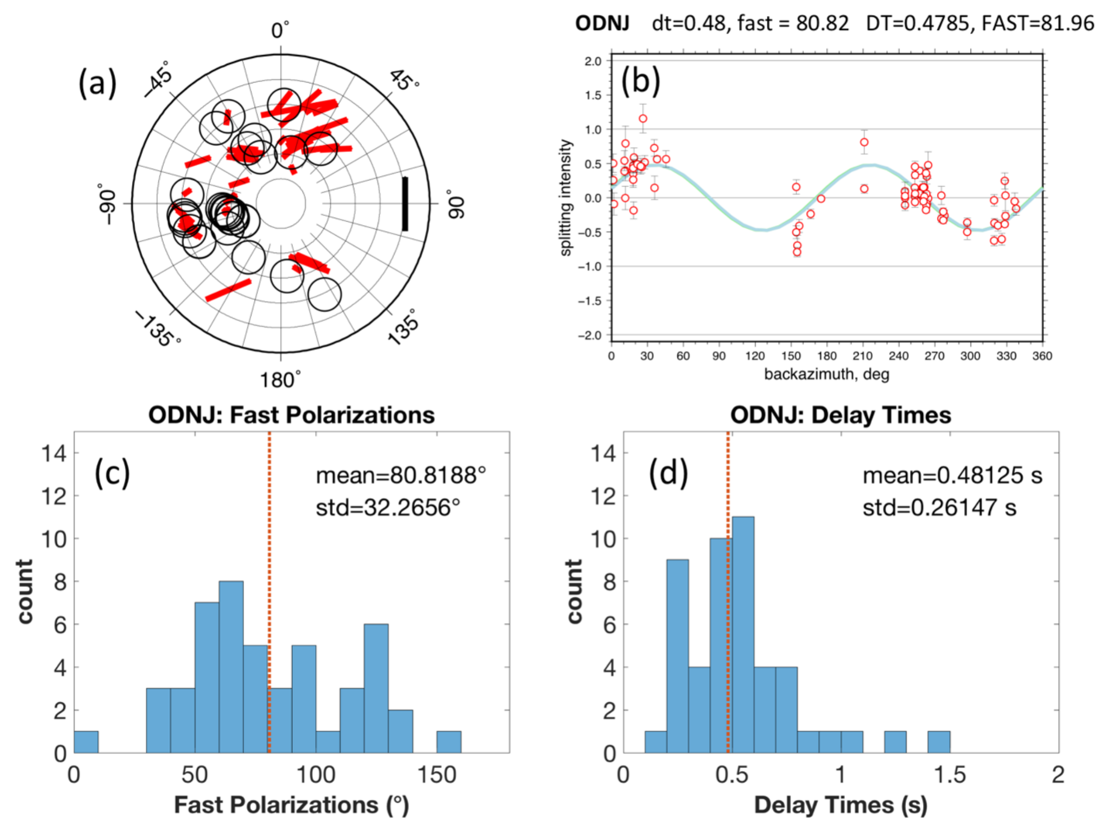

Figure A27: Station ODNJ

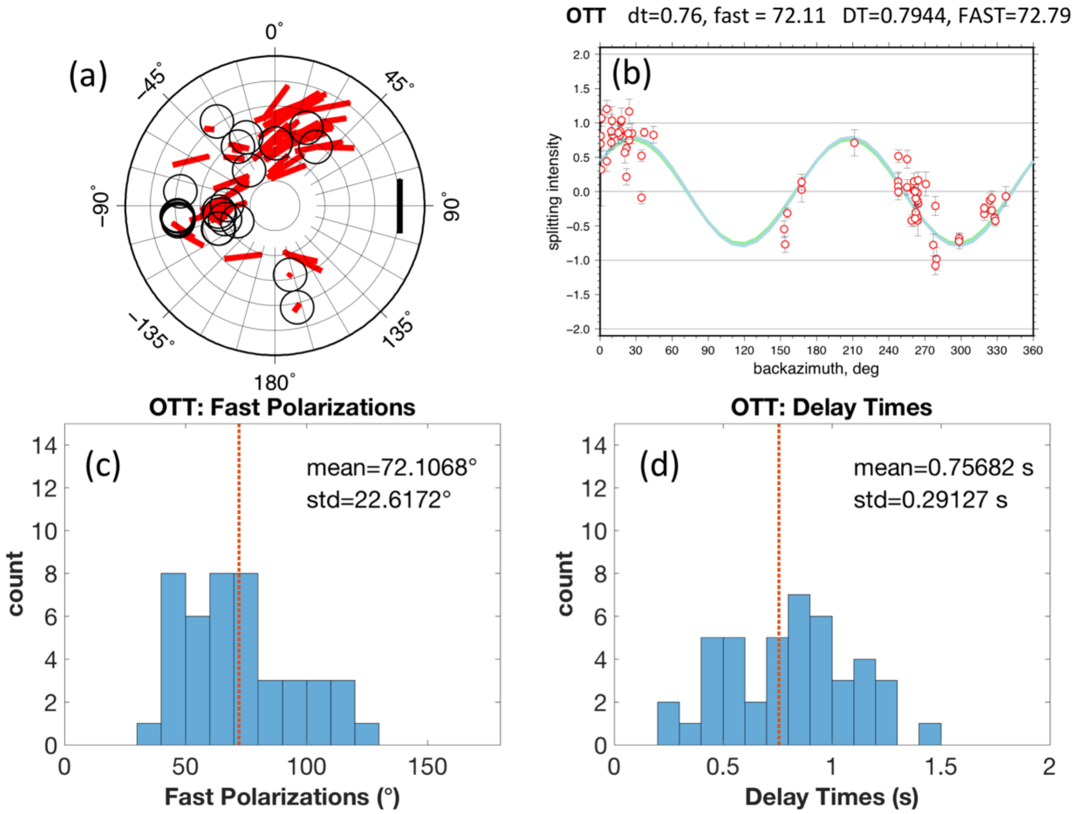

Figure A28: Station OTT

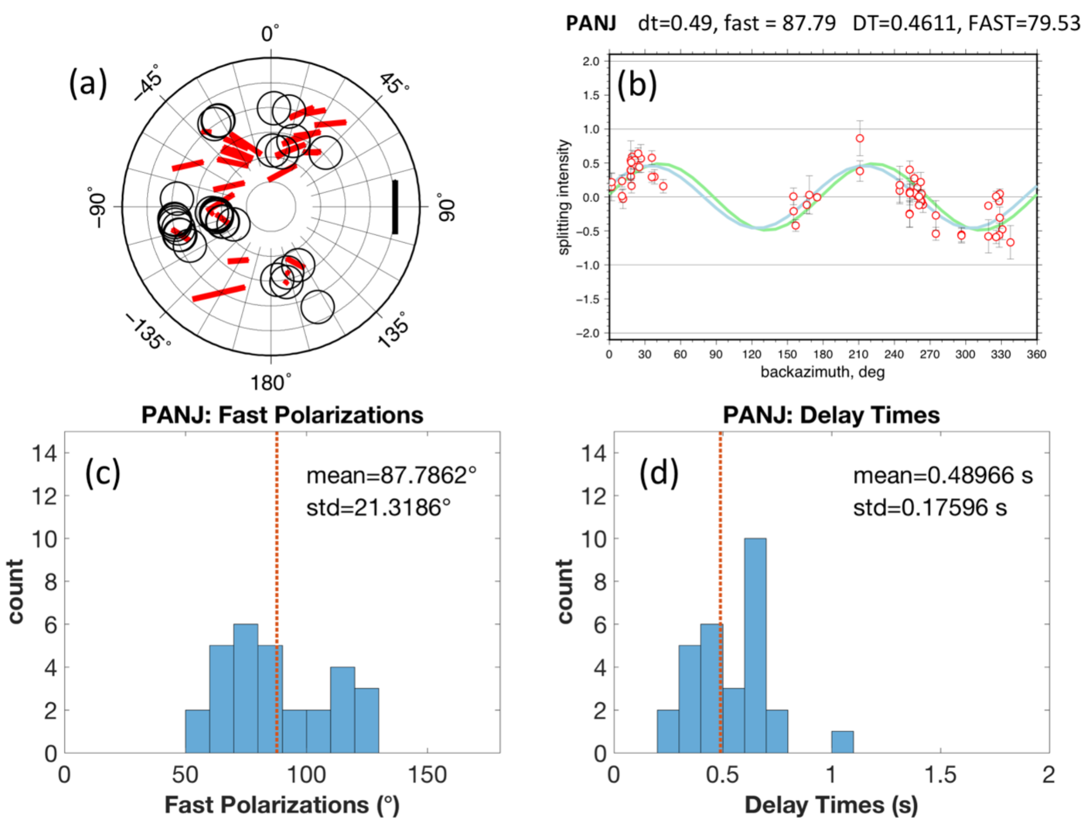

Figure A29: Station PANJ

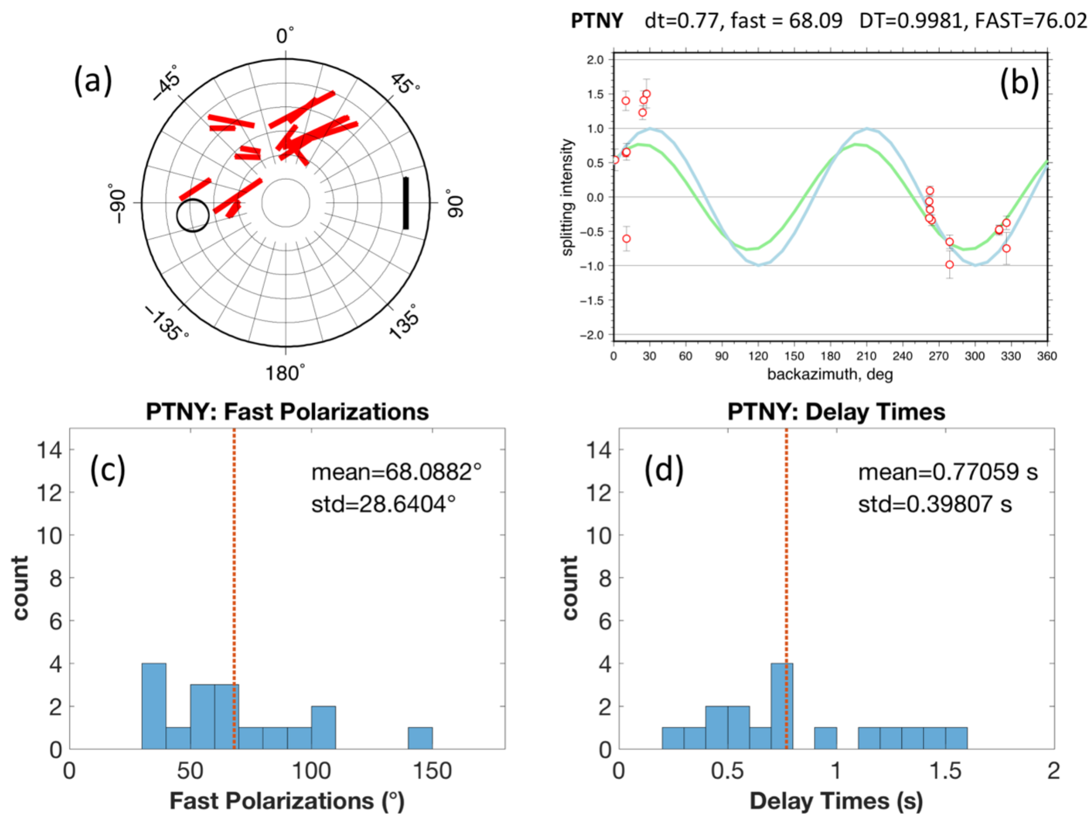

Figure A30: Station PTNY

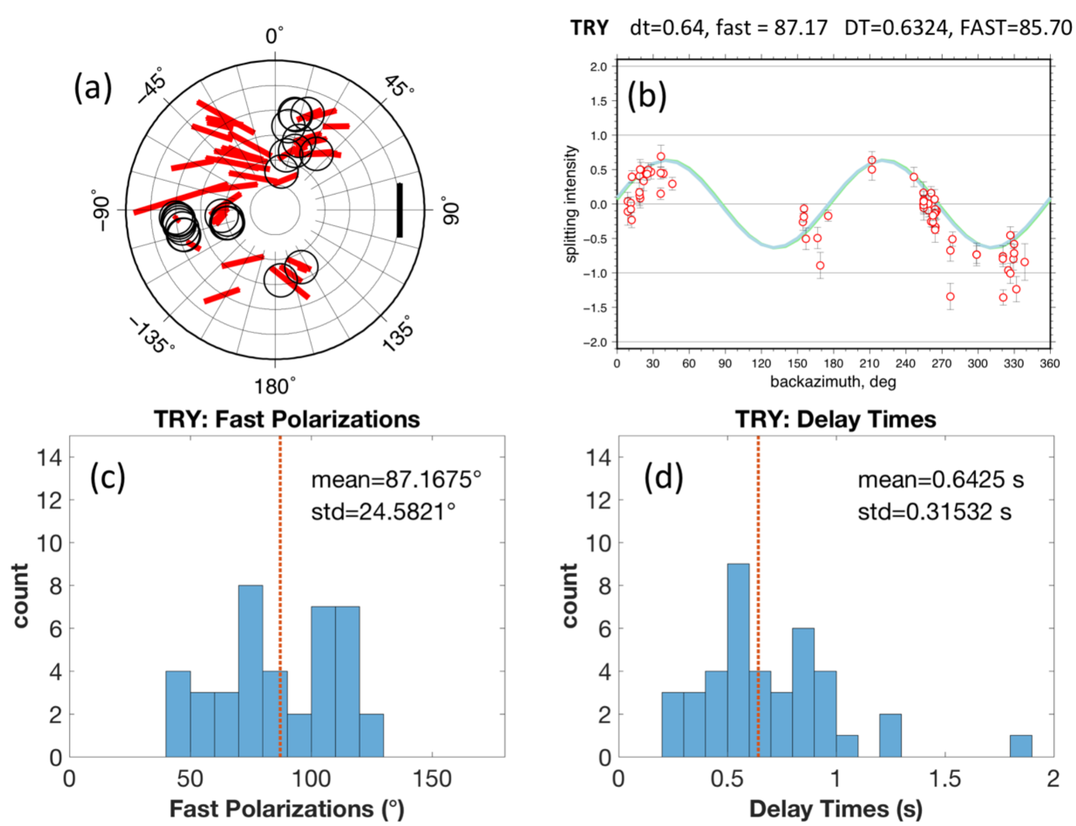

Figures A31: Station TRY

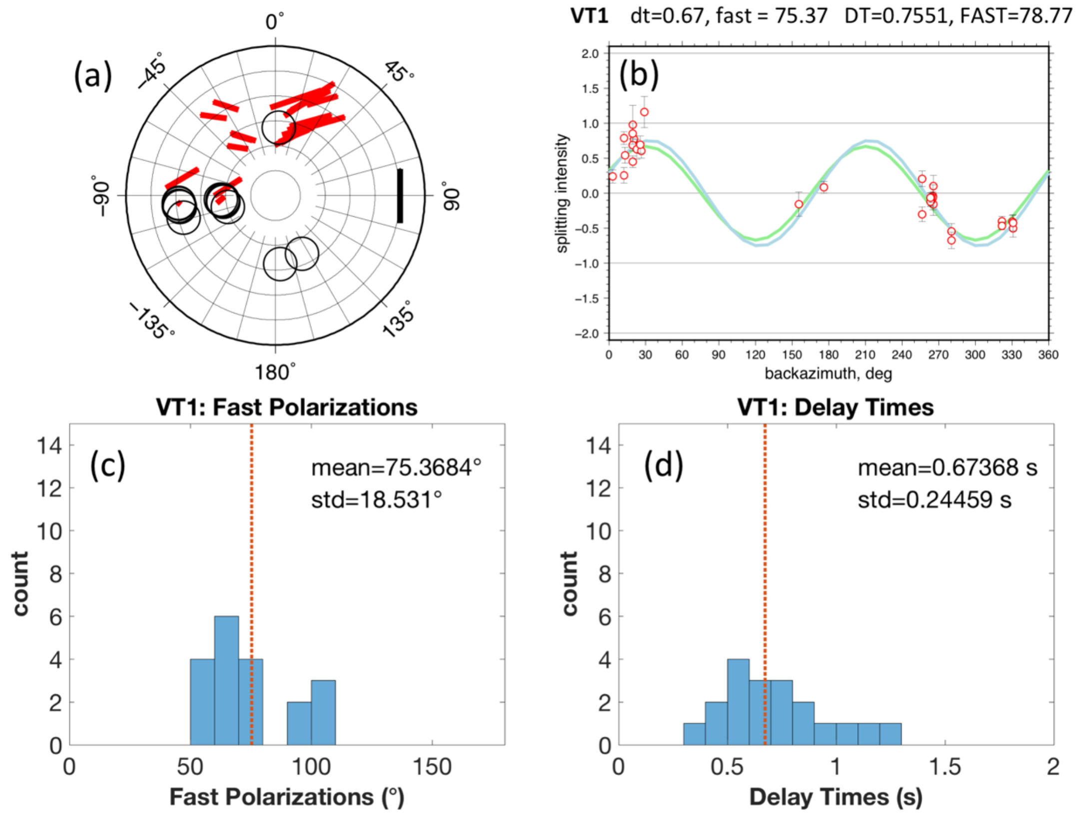

Figures A32: Station VT1

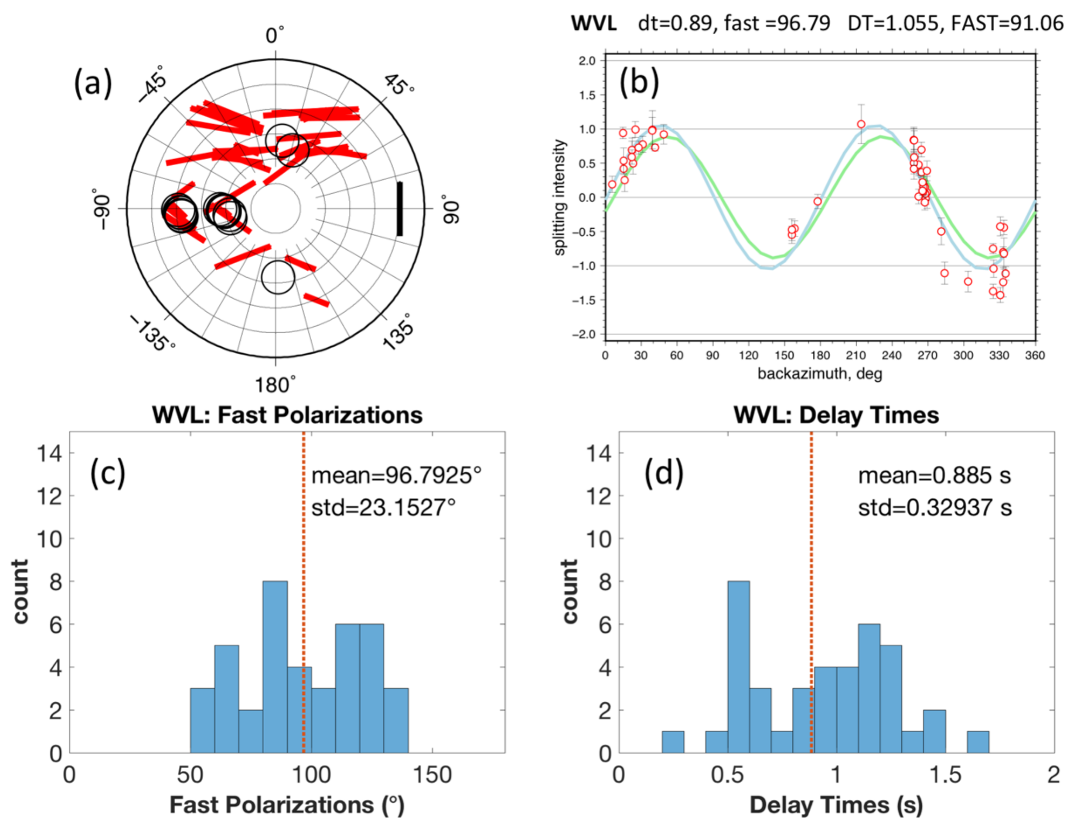

Figures A33: Station WVL

Table A1: Averaged Splitting Parameters and Statistics. Two sets of averaged splitting parameters plotted in Figure 5 of the main text. The table also includes the statistical criteria used to define the different domains, plotted in Figure 10 of the main text. The criteria include the proportion of NULL measurements in the dataset of individual stations, the standard deviation of the individual fast polarizations, and the standard deviation of the individual delay times.

Site	Latitude	Longitude	δt (SI)	φ (SI)	δt (simple)	φ (simple)	% NULL	Std. φ	Std. δt
ACCN	43.38	-73.67	0.8585	79.96	0.83	79.40	0.32	24.47	0.40
BRNJ	40.68	-74.57	0.4101	91.27	0.47	105.95	0.46	30.03	0.19
BRNY	41.41	-74.01	0.7905	80.72	0.68	77.18	0.30	22.50	0.36
D62A	47.08	-69.05	1.001	69.56	0.88	59.88	0.22	11.87	0.39
E62A	46.62	-69.52	1.145	78.51	0.75	71.23	0.13	25.74	0.37
E63A	46.42	-68.46	0.8671	85.07	0.6	84.82	0.19	28.26	0.30
F63A	45.70	-69.10	1.027	86.61	0.89	82.99	0.29	29.05	0.73
FFD	43.47	-71.65	0.2734	95.40	0.36	106.17	0.73	28.23	0.15
FRNY	44.84	-73.59	0.7886	74.84	0.72	77.32	0.26	21.71	0.37
G62A	45.22	-70.53	1.097	85.54	0.82	77.76	0.15	28.02	0.49
G65A	45.20	-67.56	1.38	74.37	1.06	72.59	0.04	24.19	0.66
H62A	44.57	-71.16	0.8441	84.37	0.77	77.08	0.29	19.35	0.35
I62A	43.87	-71.34	0.37	87.52	0.43	91.74	0.42	32.69	0.20
I63A	44.05	-70.58	0.7905	92.51	0.71	93.16	0.41	21.66	0.33
J57A	43.41	-76.00	0.7955	78.48	0.74	78.74	0.31	23.42	0.38
J59A	43.46	-74.50	1.167	72.86	0.9	66.62	0.23	22.41	0.41
J61A	43.35	-72.55	0.5187	78.61	0.63	61.86	0.40	30.98	0.33
K62A	42.67	-72.23	0.5423	89.34	0.52	85.92	0.41	22.98	0.25
L59A	42.19	-75.04	0.4913	79.92	0.55	76.71	0.43	28.47	0.25
L64A	41.94	-70.84	0.101	76.50	0.34	84.91	0.83	42.01	0.12
LATQ	47.38	-72.78	1.177	90.49	0.94	92.03	0.40	21.17	0.63
LUPA	40.60	-75.37	0.5853	96.11	0.47	90.50	0.35	29.14	0.21
M63A	41.40	-72.05	0.5826	91.13	0.54	93.42	0.40	25.75	0.22
MNTQ	45.50	-73.62	1.32	89.06	1.16	98.71	0.32	20.73	0.45
N62A	40.93	-73.47	0.8023	78.17	0.67	73.49	0.27	23.81	0.33
NPNY	41.75	-74.14	0.6111	81.06	0.55	89.50	0.42	25.81	0.26
ODNJ	41.08	-74.61	0.4785	81.96	0.48	80.82	0.39	32.27	0.28
OTT	45.39	-75.72	0.7944	72.79	0.76	72.11	0.34	22.62	0.38
PANJ	40.38	-74.70	0.4611	79.53	0.49	87.79	0.53	21.32	0.23
PTNY	44.56	-74.95	0.9981	76.02	0.77	68.09	0.11	28.64	0.43
VT1	44.32	-72.75	0.7551	78.77	0.67	75.37	0.41	18.53	0.33
WVL	44.56	-69.66	1.055	91.06	0.89	96.79	0.27	23.15	0.44
TRY	42.73	-73.67	0.6324	85.70	0.64	87.17	0.39	24.58	0.36

References

Abt, D. L., Fischer, K. M., French, S. W., Ford, H. A., Yuan, H., & Romanowicz, B. (2010). North American lithospheric discontinuity structure imaged by Ps and Sp receiver functions. *Journal of Geophysical Research*, *115*, 1–24. https://doi.org/10.1029/2009JB006914

Aragon, J., Long, M. D., & Benoit, M. H. (2017). Lateral Variations in SKS Splitting Across the MAGIC Array, Central Appalachians. *Geochemistry, Geophysics, Geosystems*, *18*, 4136–4155. https://doi.org/10.1002/2017GC007169

Bowman, J. R., & Ando, M. (1987). Shear-wave splitting in the upper-mantle wedge above the Tonga subduction zone. *Geophysical Journal of the Royal Astronomical Society*, *88*(1), 25–41. https://doi.org/10.1111/j.1365-246X.1987.tb01367.x

Chen, X., Li, Y., & Levin, V. (2018). Shear Wave Splitting Beneath Eastern North American Continent: Evidence for a Multi-layered and Laterally Variable Anisotropic Structure. *Geochemistry, Geophysics, Geosystems*, *19*. https://doi.org/10.1029/2018GC007646

Chevrot, S. (2000). Multichannel analysis of shear wave splitting. *Journal of Geophysical Research: Solid Earth*, *105*(B9), 21579–21590. https://doi.org/10.1029/2000JB900199

Crampin, S. (1977). A review of the effects of anisotropic layering on the propagation of seismic waves. *Geophysical Journal of the Royal Astronomical Society*, *49*(1), 9–27.

Deng, J., Long, M. D., Creasy, N., Wagner, L., Beck, S., Zandt, G., … Minaya, E. (2017). Lowermost mantle anisotropy near the eastern edge of the Pacific LLSVP: Constraints from SKS-SKKS splitting intensity measurements. *Geophysical Journal International*, *210*(2), 774–786. https://doi.org/10.1093/gji/ggx190

Eaton, D. W., & Frederiksen, A. (2007). Seismic evidence for convection-driven motion of the North American plate. *Nature*, *446*(March), 428–431. https://doi.org/10.1038/nature05675

Gilligan, A., Bastow, I. D., Watson, E., Darbyshire, F. A., Levin, V., Menke, W., … Petrescu, L. (2016). Lithospheric deformation in the Canadian Appalachians : evidence from shear wave splitting. *Geophysical Journal International*, *206*, 1273–1280. https://doi.org/10.1093/gji/ggw207

Gripp, A. E., & Gordon, R. G. (2002). Young tracks of hotspots and current plate velocities. *Geophysical Journal International*, *150*, 321–361.

Hatcher, R. D. (2010). The Appalachian orogen: A brief summary. *The Geological Society of America Memoir*, *206*(01), 01-19. https://doi.org/10.1130/2010.1206(01).

Hibbard, J., & Waldron, J. W. F. (2009). Truncation and translation of Appalachian promontories: Mid-Paleozoic strike-slip tectonics and basin initiation. *Geology*, *37*(6), 487–490. https://doi.org/10.1130/G25614A.1

Hynes, A., & Rivers, T. (2010). Protracted continental collision — evidence from the Grenville Orogen 1, *620*, 591–620. https://doi.org/10.1139/E10-003

Karabinos, P., Samson, S. D., Hepburn, J. C., & Stoll, H. M. (1998). Taconian orogeny in the New England Appalachians: Collision between Laurentia and the Shelburne Falls arc. *Geology*, *26*(3), 215–218. https://doi.org/10.1130/0091-7613(1998)026<0215:TOITNE>2.3.CO;2

Levin, V., Long, M. D., Skryzalin, P., Li, Y., & López, I. (2018). Seismic evidence for a recently formed mantle upwelling beneath New England. *Geology*, *46*(1), 87–90. https://doi.org/10.1130/G39641.1

Levin, V., Menke, W., & Park, J. (1999). Shear wave splitting in the Appalachians and the Urals: A case for multilayered anisotropy. *Journal of Geophysical Research*, *104*(B8), 17975–17993.

Long, M. D., Jackson, K. G., & McNamara, J. F. (2015a). SKS splitting beneath Transportable Array stations in eastern North America and the signature of past lithospheric deformation. *Geochemistry, Geophysics, Geosystems*, *17*, 2–15. https://doi.org/10.1002/2014GC005684.Key

Long, M. D., & Silver, P. G. (2009). Shear wave splitting and mantle anisotropy: Measurements, interpretations, and new directions. *Surveys in Geophysics*, *30*, 407–461. https://doi.org/10.1007/s10712-009-9075-1

Long, M. D., & van der Hilst, R. D. (2005). Estimating shear-wave splitting parameters from broadband recordings in Japan: A comparison of three methods. *Bulletin of the Seismological Society of America*, *95*(4), 1346–1358. https://doi.org/10.1785/0120040107

Mclelland, J. M., Selleck, B. W., Hamilton, M. A., & Bickford, M. E. (2010). LATE- TO POST-TECTONIC SETTING OF SOME MAJOR PROTEROZOIC ANORTHOSITE – MANGERITE – CHARNOCKITE – GRANITE (AMCG) SUITES, *48*, 729–750.

Park, J., & Levin, V. (2002). Seismic Anisotropy: Tracing Plate Dynamics in the Mantle. *Science*, *296*(5567), 485–489. https://doi.org/10.1126/science.1067319

Rychert, C. A., Rondenay, S., & Fischer, K. M. (2007). P -to- S and S -to- P imaging of a sharp lithosphere-asthenosphere boundary beneath eastern North America. *Journal of Geophysical Research*, *112*, 1–21. https://doi.org/10.1029/2006JB004619

Savage, M. K. (1999). Seismic Anisotropy What Have and From Deformation ' We Learned Shear Wave Splitting ? *Reviews of Geophysics*, *37*(1), 65–106.

Shen, W., & Ritzwoller, M. H. (2016). Crustal and uppermost mantle structure beneath the United States. *Journal of Geophysical Research: Solid Earth*, *121*, 4306–4342.

https://doi.org/10.1002/2016JB012887.Received

Silver, P. G. (1996). SEISMIC ANISOTROPY BENEATH THE CONTINENTS: Probing the Depths of Geology. *Annual Review of Earth and Planetary Sciences*, *24*(1), 385–432. https://doi.org/10.1146/annurev.earth.24.1.385

Silver, P. G., & Chan, W. W. (1991). Shear Wave Splitting and Sub continental Mantle Deformation. *Journal of Geophysical Research*, *96*(B10), 16429–16454.

Sleep, N. H. (1990). Monteregian Hotspot Track : A Long-Lived Mantle Plume Montreal . *Journal of Geophysical Research*, *95*(B13), 21983–21990.

Vinnik, L. P., Farra, V., & Romanowicz, B. (1989). Azimuthal Anisotropy in the Earth From Observations of SKS At Geoscope and Nars Broadband Stations. *Bulletin of the Seismological Society of America*, *79*(5), 1542–1558.

Wagner, L. S., Long, M. D., Johnston, M. D., & Benoit, M. H. (2012). Lithospheric and asthenospheric contributions to shear-wave splitting observations in the southeastern United States. *Earth and Planetary Science Letters*, *341–344*, 128–138. https://doi.org/10.1016/j.epsl.2012.06.020

White-gaynor, A. L., & Nyblade, A. A. (2017). Shear wave splitting across the Mid-Atlantic region of North America : A fossil anisotropy interpretation, *45*(6), 555–558. https://doi.org/10.1130/G38794.1

Wüstefeld, A., & Bokelmann, G. (2007). Null Detection in Shear-Wave Splitting Measurements. *Bulletin of the Sei*, *97*(4), 1204–1211. https://doi.org/10.1785/0120060190

Wüstefeld, A., Bokelmann, G., Zaroli, C., & Barruol, G. (2008). SplitLab: A shear-wave splitting environment in Matlab. *Computers & Geosciences*, *34*, 515–528. https://doi.org/10.1016/j.cageo.2007.08.002

Yang, B. B., Liu, Y., Dahm, H., Liu, K. H., & Gao, S. S. (2017). Seismic azimuthal anisotropy beneath the eastern United States and its geodynamic implications. *Geophysical Research Letters*, *44*, 2670–2678. https://doi.org/10.1002/2016GL071227

Yang, X., & Gao, H. (2018). Full-Wave Seismic Tomography in the Northeastern United States : New Insights Into the Uplift Mechanism of the Adirondack Mountains. *Geophysical Research Letters*, 5992–6000. https://doi.org/10.1029/2018GL078438

Zhang, S., & Karato, S. (1995). Lattice preferred orientation of olivine aggregates deformed in simple shear. *Nature*. https://doi.org/10.1038/375774a0

Geological Survey of Canada (1989): Canadian National Seismograph Network. International Federation of Digital Seismograph Networks. Other/Seismic Network. 10.7914/SN/CN

Albuquerque Seismological Laboratory (ASL)/USGS (1994): New England Seismic Network. International Federation of Digital Seismograph Networks. Other/Seismic Network. 10.7914/SN/NE

Albuquerque Seismological Laboratory (ASL)/USGS (1990): United States National Seismic Network. International Federation of Digital Seismograph Networks. Other/Seismic Network. 10.7914/SN/US

UC San Diego (2013): Central and Eastern US Network. International Federation of Digital Seismograph Networks. Other/Seismic Network. 10.7914/SN/N4

IRIS Transportable Array (2003): USArray Transportable Array. International Federation of Digital Seismograph Networks. Other/Seismic Network. 10.7914